

ATAT 1.1, an Automated Timing Accordance Tool for comparing ice-sheet model output with geochronological data

Jeremy C. Ely¹, Chris D. Clark¹, David Small² and Richard C.A. Hindmarsh³

¹Department of Geography, The University of Sheffield, Sheffield, S10 2TN, UK

²Department of Geography, Durham University, Durham, DH1 3LE, UK

³British Antarctic Survey, High Cross, Madingley Road, Cambridge, CB3 0ET, UK

Correspondence to: Jeremy C. Ely (j.ely@sheffield.ac.uk)

Abstract. Earth's extant ice sheets are of great societal importance given their ongoing and potential future contributions to sea-level rise. Numerical models of ice sheets are designed to simulate ice sheet behaviour in response to climate changes, but to be improved require validation against observations. The direct observational record of extant ice sheets is limited to a few recent decades, but there is a large and growing body of geochronological evidence spanning millennia constraining the behaviour of palaeo-ice sheets. Hindcasts can be used to improve model formulations and study interactions between ice sheets, the climate system and landscape. However, ice-sheet modelling results have inherent quantitative errors stemming from parameter uncertainty and their internal dynamics, leading many modellers to perform ensemble simulations, while uncertainty in geochronological evidence necessitates expert interpretation. Quantitative tools are essential to examine which members of an ice-sheet model ensemble best fit the constraints provided by geochronological data. We present an Automated Timing Accordance Tool (ATAT version 1.1) used to quantify differences between model results and geochronological-data on the timing of ice sheet advance and/or retreat. To demonstrate its utility, we perform three simplified ice-sheet modelling experiments of the former British-Irish Ice Sheet. These illustrate how ATAT can be used to quantify model performance, either by using the discrete locations where the data originated together with dating constraints or by comparing model outputs with empirically-derived reconstructions that have used these data along with wider expert knowledge. The ATAT code is made available and can be used by ice-sheet modellers to quantify the goodness of fit of hindcasts. ATAT may also be useful for highlighting data inconsistent with glaciological principles or reconstructions that cannot be replicated by an ice sheet model.

1 Introduction

Numerical models have been developed which simulate ice sheets under a given climate forcing (e.g. Greve, 1995; Rutt et al., 2009; Pollard and DeConto, 2009; Winkelmann et al., 2011; Gudmundsson et al., 2012; Cornford et al., 2013; Pattyn, 2017). When driven by future climate scenarios, these models are used to forecast the fate of the Antarctic and Greenland ice sheets (e.g. Seddik et al., 2012; DeConto and Pollard, 2016), providing predictions of their potential contribution to future sea level rise. However, incomplete knowledge of ice physics, boundary conditions (e.g. basal topography) and parameterisations of physical processes (e.g. basal sliding, calving), as well as the difficulty of predicting future climate, lead to uncertainty in these predictions (Applegate et al., 2012; Briggs et al., 2014; Ritz et al., 2015). Observations of ice marginal fluctuations (decades) and the processes of ice calving, flow or melting (subaerial or submarine) that facilitate or drive such variations, provide a powerful means to understand the processes leading to the possibility of deriving new formulations that improve the realism of

37 modelling. However, the short-time span (decades) of these observations limits their being used to constrain,
38 initialise or validate modelling experiments (Bamber and Aspinall, 2013). Conversely, palaeo-ice sheets,
39 especially from the last glaciation (~21,000 years ago), left behind evidence which provides the opportunity to
40 study ice sheet variations across timescales of centuries to millennia, albeit with increased uncertainty in exact
41 timing.

42 Numerous modelling studies have aimed to simulate the growth and decay of palaeo-ice sheets, producing
43 hindcasts of ice-sheet behaviour (e.g. Boulton and Hagdorn, 2006; Hubbard et al., 2009; Tarasov et al., 2012;
44 Gasson et al., 2016; Patton et al., 2016). Results from these hindcasts may be compared with empirical data
45 recording ice sheet activity, so as to discern which parameter combinations produce results that best replicate the
46 evidence of palaeo-ice sheet activity. Three classes of data are of particular use for constraining palaeo-ice sheets;
47 (i) geomorphological data, (ii) relative sea level history, and (iii) geochronological data. Ideally, all three classes
48 of data should be used to quantify the goodness of fit of a hindcast.

49 Geomorphological evidence comprises the landforms created by the action of ice upon the landscape, and can
50 typically provide data on ice extent, recorded by moraines and other ice marginal landforms and on ice-flow
51 directions recorded by subglacial landforms such as drumlins. Such landforms can be used to decipher the pattern
52 of glaciation (e.g. Kleman et al., 2006; Clark et al., 2012; Hughes et al., 2014). Two tools have already been
53 developed which can compare modelled ice margins and flow directions to the geomorphological evidence base
54 (Napieralski et al., 2007).

55 Relative sea level data provides information regarding the mass-loading history of an ice sheet. Palaeo-ice-sheet
56 model output is often evaluated against relative-sea-level data by use of glacio-isostatic adjustment models (e.g.
57 Tushingham and Peltier, 1992; Simpson et al., 2009; Tarasov et al., 2012; Auriac et al., 2016).

58 Geochronological evidence attempts to ascertain the absolute timing of ice advance and retreat using dated
59 material (e.g. organic remains dated by radiocarbon measurement) found in sedimentary contexts interpreted as
60 indicating ice presence or absence nearby. It enables reconstruction of the chronology of palaeo-ice sheet growth
61 and decay (Small et al., 2017) and is the underpinning basis for empirically-based ice sheet margin reconstructions
62 (e.g. Dyke, 2004; Clark et al., 2012; Hughes et al., 2016). Although widely used in empirical reconstruction of
63 palaeo-ice sheets, geochronological data has rarely been directly compared with ice sheet model output (although
64 see Briggs and Tarasov, 2013). Such a comparison could be useful both for constraining ice-sheet model
65 uncertainty and for identifying problems with the geochronological record. For example, a poor fit between model
66 output and empirical data on timing could inform on the validity of a numerical model (or its parameterisation),
67 or it could provide a physical basis for questioning the plausibility of empirically-driven interpretations or specific
68 lines/data points of evidence given that they are associated with inherent uncertainties. In order to maximise the
69 benefit to all users, any comparisons between palaeo-ice sheet model output and empirical data should ideally
70 consider the inherent uncertainties of both.

71 Given the wide availability of compilations of geochronological data (e.g. Dyke, 2004; Hughes et al., 2011;
72 Hughes et al., 2016), as well as the proliferation of ice sheet models (e.g. Greve, 1995; Rutt et al., 2009; Pollard
73 and DeConto, 2009; Winkelmann et al., 2011; Gudmundsson et al., 2012; Cornford et al., 2013; Pattyn, 2017), a
74 convenient, reproducible and consistent procedure for comparison should be of great utility to the palaeo-ice sheet
75 community. The typical volume of geochronological constraints (several thousands) for a palaeo ice sheet and the
76 number of ensemble runs (several hundreds) from an ice sheet model make a visual matching of data and model

77 output nearly impossible to accomplish, which is likely to explain the rarity of such comparisons. Here, we present
78 an Automated Timing Accordance Tool (ATAT, version 1.1). ATAT a systematic means for comparing ice-sheet
79 model output with geochronological data, which quantifies the degree of fit between the two. To separate model
80 uncertainty from data error, a single run of ATAT focuses on the error in geochronological data. However, through
81 multiple comparisons against an ice-sheet model ensemble which considers model uncertainty, ATAT could be
82 used as a basis for examining whether model-data mismatch is a consequence of inadequacies in either the model
83 or data. The tool is in the form of a Python script and requires the installation of open-source libraries. ATAT is
84 written to handle NETCDF data as an input, a format commonly used in ice sheet modelling and is also accessible
85 from many GIS packages in which geochronological data can be stored and manipulated.

86 **2 Background**

87 Geochronological evidence and ice sheet model outputs are often independently used to reconstruct the timing of
88 glaciological events. The two approaches are fundamentally different in nature and consequently produce
89 contrasting data outputs. Thus, before describing our approach to comparing the two sets of data (ATAT), we first
90 consider the nature of both geochronological data and ice-sheet model output to highlight the issues and potential
91 difficulties associated with comparing the two and conceptualise a comparison procedure.

92 **2.1 Geochronological data**

93 The timing of palaeo-ice sheet activity has primarily been dated using three techniques: (i) radiocarbon dating;
94 (ii) cosmogenic nuclide exposure dating, and (iii) luminescence dating (Figure 1). The utility of each method for
95 determining the timing of palaeo-ice sheet activity has been extensively reviewed elsewhere (e.g. Fuchs and
96 Owen, 2008; Balco, 2011; Small et al., 2017) and only a brief description is provided here. Radiocarbon dating
97 uses the known rate of the radioactive decay of ^{14}C to determine the time elapsed since the death of organic
98 material (Libby et al., 1949; Arnold and Libby, 1951; Figure 1). For palaeo-glaciological purposes, the dated
99 organic material (e.g. shells, mosses, plant remains) is usually taken from basal sediments overlying and closely
100 associated with a glacial deposit in order to determine a minimum deglaciation age (e.g. Heroy and Anderson,
101 2007; Lowell et al., 2009); ice is interpreted to have retreated from this site some short time prior to this age.
102 Where organic matter is either reworked within or is located directly beneath a glacial deposit, it can be used to
103 constrain the maximum age of glacial advance (e.g. Brown et al., 2007; Ó Cofaigh and Evans, 2007); advance
104 happened sometime after this age. Cosmogenic nuclides (e.g. ^{10}Be , ^{26}Al and ^{36}Cl) are produced by the
105 interaction of secondary cosmic radiation in minerals, such as quartz, within materials exposed at the Earth's
106 surface (Figure 1). Samples are generally taken from glacially-transported boulders, morainic boulders and
107 glacially modified bedrock, all of which have ideally had signals from any previous exposure history removed by
108 glacial erosion. Cosmogenic nuclide dating is thus used to determine the duration of time a sample has been
109 exposed at the Earth's surface by determination of the concentration of cosmogenic nuclides within that sample.
110 Luminescence dating can determine the age of a deposit by measuring the charge accumulated within minerals.
111 This charge accumulates in light-sensitive traps within the crystal lattice due to ionizing radiation produced by
112 naturally occurring radioactive elements (e.g. U, Th, K). Luminescence dating determines the time elapsed since
113 the last exposure of the mineral to sunlight; this exposure acts to reset the signal (Figure 1). As subglacial deposits

114 are unlikely to have been exposed to light before burial, and therefore contain signals accumulated prior to
115 deposition, luminescence dating within palaeo-glaciology is typically applied to ice marginal sediments, or those
116 which overly glacial sediments (e.g. Duller, 2006; Smedley et al., 2016; Bateman et al., 2018). All
117 geochronological techniques record the absence of grounded ice. They therefore provide either maximum or
118 minimum ages of a glaciological event, depending upon the stratigraphic setting. Table 1 outlines a commonly
119 used system used to classify geochronological data by stratigraphic setting (Hughes et al., 2011; 2016).
120 The retreat/advance (ice-free) ages provided by the three geochronometric techniques are all affected by
121 systematic and geological uncertainties (Small et al., 2017). Systematic uncertainties originate from the tools and
122 techniques used to derive the date, such as laboratory instruments and sample preparation, and are accounted for
123 in the quoted errors that accompany a date. Geological uncertainties are caused by the geological history of a
124 sample, before, during and after a glacial event (e.g. Lowe and Walker, 2000; Lukas et al., 2007; Heyman et al.,
125 2011). Such influences may leave little or no evidence of their effect upon a sample and are thus hard to quantify.
126 The relationship between a dated sample and the glacial event it indicates is the largest potential source of
127 uncertainty in geochronological data and is primarily bounded by the ability of the investigator to find and
128 associate dateable material to the glacial event of interest. Since all geochronological techniques measure the
129 absence of ice, expert inference must be made, and are influenced by the availability of information (stratigraphic
130 or otherwise) at a study site; they may be open to change (e.g. new radiocarbon calibrations, new cosmogenic
131 isotope production rates). Furthermore, in the cases of luminescence and radiocarbon dating, there can be an
132 unknown duration since glacial occupation of an area and the deposition of dateable material. These factors mean
133 it is necessary to consider the quality of dates for ascertaining the timing of the glacial event in question (Small et
134 al., 2017).
135 Numerous geochronological studies have sought to ascertain the timing of palaeo-ice sheet activity at sites, leading
136 to compilations of geochronological data which bring together hundreds to thousands of published dates (e.g.
137 Dyke et al., 2002; Livingstone et al., 2012; Hughes et al., 2011; 2016). Despite the growing number of reported
138 dates, they are still insufficient in number and spatial spread to define, on their own, the time-space envelope of
139 the shrinking ice sheet. Techniques to interpolate geochronological information between sites are required. The
140 most commonly used technique is empirical ice sheet reconstruction (e.g. Dyke, 2004; Clark et al., 2012), whereby
141 expert assessments of the geochronological and geomorphological record are used together to create ice-sheet
142 wide isochrones of ice-sheet margin position and flow configuration. A recent advance in this method has been
143 the inclusion of confidence envelopes for each isochrone, documenting possible maximum, likely and minimum
144 extents (Hughes et al., 2016). Further techniques for spatiotemporally interpolating geochronological data include
145 Bayesian sequence modelling (e.g. Chiverrell et al., 2013; Smedley et al., 2017), in which collections of deglacial
146 ages are arranged in spatial order determined by a priori knowledge of geomorphologically-informed ice flow and
147 retreat patterns (e.g. Gowan, 2013). Such techniques provide viable methods for producing ice-sheet wide
148 chronologies, filling in information in locations where geochronological data may be sparse.

149 **2.2 Ice sheet model output**

150 Ice-sheet models solve equations for ice flow over a computational domain, for a given set of input parameters
151 and boundary conditions, to determine the likely flow geometry and extent of an ice sheet. Typically, ice-sheet
152 models run using finite difference techniques on regular grids (e.g. Rutt et al., 2009; Winkelmann et al., 2011).

153 Ice-sheet models that utilise adaptive meshes (e.g. Cornford et al., 2013) and unstructured meshes also exist (e.g.
154 Larour et al., 2012) and the results from such models can be interpolated onto spatially regular grids. The spatial
155 resolution of an ice-sheet model depends upon the computational resources available, and the spatial resolution
156 of available boundary conditions. Continental-scale models of palaeo-ice sheets have typical spatial resolution of
157 tens of kilometres (e.g. Briggs and Tarasov, 2013; DeConto and Pollard, 2016; Patton et al., 2016), though parallel,
158 high-performance computing means higher resolutions are possible (e.g. 5 km in Golledge et al., 2013 and
159 Seguinot et al., 2016). The temporal resolution of ice sheet model output is ultimately limited by the time-steps
160 imposed by the stability properties of the numerical schemes solving the ice-flow equations. Given that these
161 stable time-steps can be sub-annual, output frequency is mostly predetermined by the user (typically decades to
162 centuries), and as such is constrained by available disk-storage. Ice-sheet models therefore produce spatially
163 connected predictions of ice-sheet behaviour such as advance and deglaciation (e.g. Table 1) across gridded
164 domains at various temporal and spatial resolutions.

165 The stress fields imposed upon ice can be fully described by solving the Stokes equations. Indeed, ‘full Stokes’
166 models which do so have been tested (Pattyn et al., 2008) and used to simulate ice sheets (e.g. Seddik et al., 2012).
167 However, fully solving the Stokes equations over the spatio-temporal scales relevant to palaeo-ice sheet
168 researchers remains beyond the limit of currently available computational power. This problem is exacerbated by
169 the need to run multi-parameter valued ensemble simulations to account for model uncertainty over multi-
170 millennial and continental-scale domains. This means that palaeo-ice sheet modelling experiments rely upon
171 approximations of the Stokes equations (see Kirchner et al., 2011 for a discussion), such as the shallow ice
172 approximation (SIA) and shallow shelf approximation (SSA). The choice of ice-flow approximation used within
173 a model has implications for the capability of models to realistically capture aspects of ice sheet flow (Hindmarsh,
174 2009; Kirchner et al., 2011; 2016), and in turn influences the nature of the model output produced. For instance,
175 the SIA is not applicable for ice shelves, therefore SIA-based models do not produce modelled ice shelves (e.g.
176 Glimmer; Rutt et al., 2009). Therefore, the timing of deglaciation in an SIA model can be determined as the point
177 at which ice thickness in a cell becomes zero or thinner than the flotation thickness, whereas in a SSA or higher-
178 order model the location and movement of the grounding line must be determined.

179 Though ice sheet models produce output which is consistent with model physics, there are many sources of
180 uncertainty involved with ice sheet modelling. This uncertainty has two main sources: (i) parameterisations, and
181 (ii) boundary conditions. Where a process is too complex (e.g. calving) or occurs at too small a scale (e.g.
182 regelation) to be captured by an ice sheet model, it is often simplified and parameterised. Associated with each
183 parameterisation are a set of parameters, the values of which are either unknown, or thought to vary within some
184 plausible bounds, and which can either be constant or spatially and temporally variable across a domain. An
185 example of a process which is often parameterised is basal sliding. This parameterisation is often done through
186 the implementation of a sliding law (e.g. Fowler, 1986; Bueler and Brown, 2009; Schoof, 2010), which relates the
187 basal shear stress to the basal velocity (Fowler, 1986). Parameters used to determine this relationship are often
188 assigned or incorporated within a parameter, or prescribed by another model parameterisation (e.g. a subglacial
189 hydrology model). Adding to the uncertainty in the absence of a single preferable sliding law, ice-sheet models
190 often allow the user to choose between different sliding law implementations.

191 Boundary conditions, the values prescribed at the edge of the modelled domain, also introduce uncertainty into
192 ice-sheet models. For contemporary ice sheets, there is a large uncertainty in the basal topography (e.g. Fretwell

193 et al., 2013). This is less of a problem for the more accessible beds of palaeo-ice sheets. However, accurately
194 accounting for the evolution of this bed topography over the course of a glaciation requires a model of isostatic
195 adjustment (Lingle and Clark, 1985; Gomez et al., 2013).

196 A very large source of uncertainty for modelling palaeo-ice sheets is the climate used to drive them (Stokes et al.,
197 2015), as indeed is the case for forecasts of contemporary ice sheets (e.g. Edwards et al., 2014). Owing to the
198 computational resources required and technical challenges, few palaeo-ice sheet models are coupled with climate
199 models. This uncertainty over past climate is reflected in the large range of outputs produced by global circulation
200 models which have tried to simulate the last glacial cycle (e.g. Braconnot et al., 2012). Palaeo-ice sheet modellers
201 have used a range of methods to force their models, including simple parameterisations (Boulton and Hagdorn,
202 2006), applying offsets derived from ice core records to contemporary climate (Hubbard et al., 2009) and scaling
203 between present-day conditions and uncoupled global-circulation-model simulations at maximum glacial
204 conditions (Gregoire et al., 2012; Gasson et al., 2016). Each approach is associated with an inherent uncertainty.
205 When this uncertainty is accounted for, the range of possible climates produces numerous ice sheet outputs.

206 There is another cause of ice-sheet models not being able to accurately predict the evolution of ice-sheets, which
207 is the presence of instabilities – we use this term in the technical sense of a small perturbation in leads to the whole
208 ice-sheet system amplifying this small perturbation to the extent it can leave a mark in the geological record. A
209 classic example of this in ice-sheet dynamics is the marine ice-sheet instability (MISI), first discussed in the 1970s
210 (Hughes, 1973; Weertman, 1974, Mercer, 1978) and more recently put on a sounder mathematical footing (Schoof
211 2007, 2012).

212 The MISI actually refers to an instability in grounding-line (GL) position on a reverse slope, where the water
213 depth is shallowing in the direction of ice flow. Since ice flux increases with ice thickness, a straightforward
214 argument leads to the conclusion that if the GL advances into shallower water, the efflux will decrease, the ice
215 sheet will gain mass and the advance continue. If, on the other hand, the GL retreats, the flux will increase, the
216 ice-sheet will lose mass and the retreat continue. In principle, given the right parameterisations and basal
217 topography, ice-sheet models should be able to predict the ‘trajectory’ of GL migration arising as a consequence
218 of the MISI. However, the MISI is one of the class of instabilities that lead to poor predictability; certain small
219 variations of parameters and specifications will lead to large-scale changes in the ‘trajectory’, in this case the
220 retreat history. A well-known analogy is the ‘butterfly effect’, which originated in atmospheric modelling work
221 (Lorenz, 1963); the butterfly effect is concerned with the consequences of the statement “small causes can have
222 larger effects”. Recent work has also shown that additional physical processes, such as ice-shelf buttressing
223 (Gudmunsson, 2012) and the effect that the gravitational pull of ice-sheets has on sea level (Gomez et al., 2012)
224 have additional effects on grounding line stability. Given that most of the palaeo-ice sheets during the last glacial
225 cycle had extensive marine margins and overdeepened basins, with isostatic adjustment creating further zones of
226 reverse slope, capturing grounding line processes is important for simulating these ice-sheets.

227 **2.3 Considerations when comparing geochronological data and ice-sheet model output**

228 Sections 2.1 and 2.2 make it clear that several factors must be considered in order to satisfactorily compare
229 geochronological data and ice-sheet model output (Table 2). Most critically, the two datasets involved in any
230 comparison have varying spatial properties. Raw geochronological data is unevenly distributed and located at
231 specific points, with horizontal position accurate to a metre or so; such data may be used to plot ice-margin

232 fluctuations of the order of tens of kilometres (Figure 2C). Ice-sheet models typically produce results on evenly-
233 spaced points (at ~5 km to 20 km resolution) that are distributed over and beyond the maximum area of the palaeo-
234 ice sheet (Table 2; Figure 2B). Consequently, in comparing the two, a choice must be made; either
235 geochronological data should be gridded (coarsened) to the resolution of the ice-sheet model, or the ice-sheet
236 model results must be interpolated to a higher resolution. Both options have drawbacks, as the former removes
237 spatial accuracy from geochronological data while the latter relies upon interpolation beyond model resolution
238 and, more seriously, model physics. A second problem lies in the spatial organisation of the data (Table 2). Ice-
239 sheet models produce a regular grid of data (Figure 2B), meaning that no location is more significant than any
240 other when comparing the modelled deglacial chronology with that inferred from geological data. Conversely,
241 owing to the uneven distribution of raw geochronological data, some regions of a palaeo-ice sheet may be better
242 constrained than others (Figure 2C). As noted by Briggs and Tarasov (2013), any comparison that does not treat
243 the uneven spatial distribution of geochronological data may favour sites where numerous dates exist over more
244 isolated locations. One approach to overcoming these disparities is to use an interpolation scheme (e.g. empirical
245 reconstruction, Bayesian sequence) on the raw geochronological data. This produces a geochronological
246 framework by combining evidence on pattern and timing to yield a distribution that is spatially more uniform and
247 a spatial resolution similar to that of palaeo-ice sheet model output (Figure 2D).

248 The temporal intervals between and precision of geochronological data and ice sheet model output also vary
249 (Table 2). The time intervals between geochronometric data are determined by the number of available
250 observations, and precision determined by sources of uncertainty. Conversely, ice sheet models produce output at
251 regular intervals and are temporally exact, which is to be contrasted with ‘correct’. Since the output interval of an
252 ice-sheet model is generally determined by the user (see Section 2.2) it is pertinent to consider an appropriate
253 time-interval of ice-sheet model output for comparison with geochronological data. For example, radiocarbon
254 dates have precision typically in the order of hundreds of years but do not directly constrain ice extent, whilst
255 empirically reconstructed isochrones are typically produced for thousand-year time-slices (e.g. Hughes et al.,
256 2016). In reality, ice-sheets may respond to events at faster time-scales than this, but in the absence of internal
257 instabilities (e.g. MISI) palaeo-ice sheet models are ultimately limited by the temporal resolution of the available
258 climate forcing data. Thus, to gain insight into controls on palaeo-ice sheet behaviour, it may be necessary to
259 create model output with a greater (centurial) temporal resolution than the uncertainty associated with
260 geochronology.

261 Both geochronological data and ice-sheet model output have sources of uncertainty which must also be considered
262 when comparing the two. For geochronological data, uncertainty is typically expressed as a standard deviation
263 from the reported age, and are therefore easy to consider when comparing to an ice sheet model. For ice-sheet
264 models, individual model runs do not currently express uncertainty, and it is only when multiple, ensemble, runs
265 which systematically vary parameters and boundary conditions are conducted that uncertainty in all output
266 variables can be expressed. Having said this, statistical techniques exist to derive probability distribution functions
267 for individual quantities (e.g. Ritz et al., 2015). Such ensemble runs typical comprise hundreds to thousands of
268 individual runs (Tarasov and Peltier, 2004; Robinson et al., 2011). Given the volume of data this produces, one
269 appealing application of a quantitative comparison between geochronological data and ice sheet model output
270 would be to act as a filter for scoring ice-sheet model runs and reducing predictive uncertainty by only using the
271 parameter combinations that were successful. However, if all possible parameters have been modelled, (i.e. the

272 full 'phase-space' of the model has been explored (cf. Briggs and Tarasov, 2013)), and very few (or no) model
273 runs conform to a certain set of geochronological data or an empirical reconstruction, this may provide a basis to
274 question aspects of the evidence (e.g. re-examining the stratigraphic context of a dated sample site or questioning
275 the basis of the reconstructed isochrone). Of course, a third possibility that both data and model are incorrect
276 cannot be excluded.

277 We therefore suggest that any comparison between ice-sheet model experiments and geochronological data should
278 consider:

- 279 i) That both ice-sheet models and geochronological data have inherent uncertainties;
- 280 ii) That geochronological data typically provide a constraint on just the absence of ice; such that ice must have
281 withdrawn from a site sometime (50 years? 500 years? 5000 years?) prior to the date (which can be any point
282 within the full range of the stated uncertainty). It is thus a limit in time and not a direct measure of glacial activity.
283 Figure 3 illustrates this for advance and retreat constraints. It is most often the case that dated material is taken
284 close to the stratigraphic boundary or landform representing ice presence, in which case a date might be considered
285 as a 'tight constraint' (e.g. the ice withdrew and very soon afterwards (50 years) marine fauna colonised the area
286 and deposited the shells used in dating). Sometimes however there may have been a large (centuries to millennia)
287 interval of time between the withdrawal and the age of the shell chosen as a sample, in which case the date will
288 provide a 'loose' limiting constraint; it might be much younger than ice retreat (Figure 3).
- 289 iii) There is inherent value to the expert interpretation of stratigraphic and geomorphological information, meaning
290 an ice-free age reported for a site is likely as close as possible (tight constraint) to a glacial event. However, this
291 interpretation could be subject to change;
- 292 iv) Geochronological data exist as spatially distributed dated sites (e.g. Figure 2C) which can be built into a
293 spatially coherent reconstruction (e.g. Figure 2D);
- 294 v) A great input uncertainty in a palaeo-ice sheet model is the climate, which can lead to changes in the spatial
295 extent and timing of ice sheet activity.
- 296 vi) A factor which requires further investigation is the relationship between the operation of a physical instability
297 (e.g. the MISI) and the practical ability of models to predict retreat or advance rates; the presence of an instability
298 can result in extreme sensitivity to parameter ignorance or over-simplified model physics.
- 299 vii) Other uncertainties can also lead to variations in ice-sheet model results; these can be accounted for in an
300 ensemble of hundreds to thousands of simulations.

301 Given the above, it is unlikely that a single procedure could capture model-data conformity. ATAT therefore
302 implements several ways of measuring data-model discrepancies and produces output maps (described in the
303 following two sections) to help a user assess which model runs best agree with the available geochronological
304 data. One approach is to transform the geochronological data points (x,y,t) to a gridded field (raster) that define
305 age constraints of ice advance and another grid for retreat. Both of these data types also require an associated grid
306 that reports the uncertainty range as error (Figure 4). These age grids may then be quantitatively compared to
307 equivalent grids (age of advance grid and age of retreat grid) derived from the ice sheet model outputs.
308 Alternatively, one might prefer to compare model runs against the geochronological data (points) combined with
309 expert-sourced interpretive geomorphological and geological data, in which age constraints from dated sites have
310 been spatially extrapolated using moraines and the wider retreat pattern. In this case ATAT allows the model

311 outputs to be compared to the ‘lines on maps’ type of reconstruction subsequent to conversion from age isolines
312 to a grid of ages (Figure 4).

313 **3. Description of tool**

314 ATAT is written in Python, and utilises several freely available modules. Access to these modules may require a
315 Python package manager, such as ‘pip’ or ‘anaconda’. ATAT can therefore be run from the command line on any
316 operating system, or by using a Python interface such as IDLE.

317 **3.1 Required data and processing**

318 ATAT requires two datasets as an input: (i) an ice-sheet model output; and (ii) gridded geochronological data.
319 Table 3 provides the required variables and standard names for each dataset. In order to determine the advance
320 age or deglacial age predicted by the ice sheet model, ATAT requires either an ice thickness (where the model
321 does not produce ice shelves) or a grounded ice-mask variable (where ice shelves are modelled). In the latter case,
322 the user is asked to define the value which represents grounded ice.

323 Empirical advance and deglacial geochronological data (Table 1) require separate input files (NETCDF format),
324 as model-data comparison for these two scenarios are run separately in ATAT. Table 1 and further references
325 (Hughes et al., 2011; 2016; Small et al., 2017), provide information regarding identification of the stratigraphic
326 setting of these two glaciological events as considered by ATAT. ATAT requires that geochronological data
327 (advance or deglacial) are interpolated onto the same grid projection and resolution as the ice-sheet model before
328 use. Though an imperfect solution to the problem of comparing grids of different resolution, (Section 2.3; Table
329 2), this was preferred to the alternative solution of regriding an ice sheet model onto a higher resolution grid, as
330 this may introduce the false impression of high resolution modelling sensitive to boundary conditions (e.g.
331 topography) beyond the actual model resolution.

332 Preparation of the geochronological data to be the same format and grid resolution as the ice sheet model output
333 requires use of a GIS software package such as ESRI ArcMap or QGIS. Users must define deglacial/advance ages
334 based either upon the availability of geochronological data in a cell, or based upon an empirical reconstruction
335 (Figure 4). These ages must be calibrated to a calendar which is the same as that output by the ice-sheet model (in
336 our case the 365-day calendar in units of seconds since 1-1-1). Where there are no data (i.e. outside the ice-sheet
337 limit), the grid value must be kept at 0. When multiple dates are contained within a cell, expert judgement is
338 required to ascertain which date is most representative of the deglaciation of a region. The assembly of this
339 geochronological database input into ATAT should consider the reliability of ages, removing outliers and
340 unreliable ages (see Small et al. (2017) for a discussion of this issue). In a comparable manner, the attribution of
341 error to each cell is also reliant upon expert interpretation. The magnitude of error may vary between the source
342 of geochronological data and user choice for experimental design (e.g. 1, 2 or 3 sigma). A single error value must
343 be given for each dated cell, corresponding to the maximum threshold beyond which it is unacceptable for a model
344 prediction to occur (Figure 3). Given that creating this input data may involve many expert decisions (e.g. which
345 date has the relevant stratigraphic setting, which date(s) are most reliable?), this part of the process is not yet
346 automated within ATAT. This data preparation stage is therefore the most time-consuming and user-intensive part
347 of the process. However, users only need to define the data-based advance/deglacial grid once to compare to

348 multiple model outputs. Future work should consider alternatives means of choosing dates and identifying outliers,
349 such as Bayesian age modelling (e.g. Chivverell et al., 2013). The input data NetCDF file should also contain the
350 variables latitude, longitude, base topography (the topography that the ice-sheet modelling is conducted on and
351 the elevation of the geochronological sample (Table 3).

352 ATAT is called from a suitable python command-line environment, using several system arguments to define
353 input variables (Table 1; Figure 5). Users must define whether they are testing a deglacial or advance scenario.
354 ATAT only considers the last time that ice advances over an area. Therefore, caution must be undertaken when
355 defining advance data in regions where multiple readvances occur, and users should consider limiting the time
356 interval of the ice sheet model tested when examining specific events (e.g. a well-dated readvance or ice sheet
357 build-up). The location of the file containing the geochronological data grid (e.g. Figure 5) is then required. From
358 this file, the age and error grids are converted to arrays. For the age data, null values are masked out using the
359 numpys masked array function. A second array that accounts for error is then created, the properties of which
360 depends upon whether a deglacial or advance scenario is being tested. For a deglacial scenario, a model prediction
361 will be unacceptable if the cell is ice-covered after the range of the date error is accounted for, but the cell may
362 become deglaciaded any time before this. Therefore, the associated error value is added onto the cell date, to create
363 a maximum age at which a cell must be deglaciaded by to conform to the ice sheet model (Figure 3). The opposite
364 is true for advance ages; ice can cover a cell any time after the date and associated error, but cannot cover the cell
365 before the date of the advance. In order to allow for advances which occur after the date and its error, associated
366 error is therefore subtracted from the date cell (Figure 3). To account for the uneven spatial distribution of dates,
367 a weighting for each date is then calculated based upon their spatial proximity. This weighting is used later when
368 comparing the data to the model output. To calculate this weighting (w_i), ATAT defines a local spatial density of
369 dated values based upon a kernel search of 10 neighbouring cells.

370 The user must define the path to the ice sheet model output, from which the modelled deglacial age will be
371 calculated and eventually compared to the data (Figure 4). The user must also define whether to base deglacial
372 timing on an ice thickness or grounded extent mask variable (Table 2). If the user selects thickness, the margin is
373 defined by an increase from 0 ice thickness. For the mask, the user is also asked to supply the number which refers
374 to grounded ice extent. The timing of advance is then determined by the change of a cell to this number (Figure
375 5). The margin position recreated by the ice-sheet model has a spatial uncertainty due to downscaling issues and
376 fluctuations which may occur between recorded outputs. To account for this, ATAT calculates a second set of
377 modelled deglacial ages, whereby the deglaciaded region at each modelled time output is expanded to all cells
378 which neighbour the originally identified deglaciaded or advanced over cells. Furthermore, the spatial resolution
379 of ice-sheet models typically means that the emergence of ice-free topography at the edge or within an ice-sheet
380 (e.g. in situations such as steep-sided valleys or nuntaks) are poorly represented. To account for this, ATAT firstly
381 calculates the modelled ice-sheet surface at each time output by adding ice thickness to the input base topography.
382 Where the modelled surface elevation is below that of the sample elevation, these cells are identified as being
383 deglaciaded (Figure 5). The downscaling of topography onto ice-sheet model grids also introduces a vertical
384 uncertainty. This is accounted for in ATAT through calculating the difference between sample elevation and the
385 reference elevation. A second metric which identifies cells as having been deglaciaded if they are also within this
386 vertical uncertainty is also calculated (Figure 5).

387 3.2 Model-data comparison

388 Once the required variables have been retrieved from the NETCDF data and manipulated, ATAT compares the
389 geochronological age and modelled age at each location (Figure 4). Firstly, the grid cells which have data are
390 categorised as to whether there is model-data agreement, based on the criteria shown in Figure 3. Since all dating
391 techniques only record the absence of ice, geochronological data provides only a one-way constraint on palaeo-
392 ice sheet activity. For deglacial ages, deglaciation could occur any time before the geochronological data provided
393 and within the error of the date, but deglaciation must not occur after the error of the date is considered (Figure
394 3). For advance ages, advance must have happened after the date or within error beforehand, but palaeo-ice sheet
395 advance cannot occur in the time period before that dated error (Figure 3). Once ATAT has determined whether
396 each cell conforms to these criteria, a map is produced identifying at which locations the ice sheet model agrees
397 with the geochronological data.

398 Though the criteria described above and illustrated in Figure 3 allow for the identification of dates which conform
399 to the predictions of an ice sheet model, they provide little insight into how close the timing of the model prediction
400 is to the geochronological data. If these were the only criteria on which a model-data comparison was made, it
401 could prove problematic. In an extreme case, one could envisage that all retreat dates are adhered to by a model
402 run that deglaciates from a maximum extent implausibly rapidly (say 50 years!), and, given that we only have
403 one-way constraints on deglaciation (Figure 3), this model run would conform to all modelled dates. Whilst the
404 nature of geochronological data (being only able to determine the absence of ice) does not preclude such a
405 scenario, this assumes that there is no inherent value to the expert judgement and stratigraphic interpretation of
406 each date as being close to palaeo-ice sheet timing (cf. Small et al. 2017). Therefore, ATAT also determines the
407 temporal proximity of the geochronological data and the model prediction. Firstly, a map of the difference between
408 modelled and empirical ages is created (Figure 5). This enables the identification of dates which are a large
409 distance away from the model prediction. Secondly, the route-mean square error (RMSE) is calculated using the
410 Eq. (2):

$$411 \quad RMSE = \sqrt{\frac{1}{n} \sum_{i=1}^n (g_i - m_i)^2},$$

412 (1)

413 where n is the number of cells which contain empirical geochronological information, g_i is the associated
414 geochronological date, and m_i is the model predicted age. The RMSE works well when the geochronological
415 data is evenly spatially distributed, either from a reconstruction (i.e. isochrones) or a wealth of dates. ATAT also
416 calculates a weighted RMSE (wRMSE), for situations where this is not the case (i.e. there is a paucity of dates
417 that are not distributed evenly across the domain) using Eq. (3):

$$418 \quad wRMSE = \sqrt{\frac{1}{n} \sum_{i=1}^n ((g_i - m_i)/w_i)^2},$$

419 (2)

420 where w_i is the spatial weighting factor. Both the RMSE and wRMSE are calculated for all dates, to create a
421 metric that doesn't account for dating error but may give an indication of how close a model-run gets to dated
422 cells, and also for those dates which where model-data agreement within dating error occurs to create a metric
423 which does account for model-error (Figure 5). ATAT then produces a .csv file containing all calculated statistics

424 per ice-sheet model output file. Given the complexity of data-model comparison, different statistics may have
425 different uses. For instance, the percentage of covered dates may prove useful to identify the worst performing
426 model runs (i.e. the bottom 50%), whilst the wRMSE of dates within error may be more convenient for choosing
427 between model runs. However, given the uncertainty in ice-sheet modelling it is likely that in an ensemble there
428 will be no single model run which has significantly better metrics than others, so ATAT may best be used to
429 choose members which pass a user-defined threshold of combined metrics.

430 **4. Application of tool**

431 **4.1 Ice Sheet Model**

432 To trial ATAT we used geochronological data and ice sheet modelling experiments from the former British-Irish
433 Ice Sheet (BIIS). A vast quantity of previous research has produced a high density of dates (Hughes et al., 2011)
434 which are being substantially augmented by the BRITICE-CHRONO project ([http://www.britice-
435 chrono.group.shef.ac.uk/](http://www.britice-chronology.group.shef.ac.uk/)). Along with an abundance of well documented landforms (Clark et al., 2017), this
436 makes the BIIS a data-rich study area for empirical reconstructions and ice sheet modelling. Ongoing modelling
437 work aims to capture the behaviour of the BIIS inferred from the geomorphological and geochronological record
438 (see Clark et al., 2012 for a recent reconstruction). We do not expect our model to capture these specific details.
439 Instead, the purpose of modelling in this paper is merely to illustrate the use of ATAT. We therefore restrict
440 ourselves to simplified modelling experiments and show only three model runs (Experiments A, B and C), whereas
441 a full ensemble experiment would contain hundreds or thousands of simulations.

442 Ice sheet modelling experiments were conducted using the Parallel Ice Sheet Model (PISM; Winkelmann et al.,
443 2011). This is a hybrid SIA-SSA model, with an implementation of grounding line physics. It is therefore suited
444 to modelling both the marine-based portions of the BIIS and the terrestrial realm. The model simulates the history
445 of the BIIS from 40 ka to present. The model is run at 5 km resolution, with basal topography derived from the
446 General Bathymetric chart of the Oceans (www.gebco.net). This is updated to account for isostatic adjustment
447 using a viscoelastic Earth model (Bueler et al., 2007) and a scalar eustatic sea level offset based on the SPECMAP
448 data (Imbrie et al., 1984). All three model runs, labelled A-C, had the same input parameters and boundary
449 conditions, apart from climate forcing. We take a similar approach to Seguinot et al. (2016) in computing a climate
450 forcing. Modern values of temperature and precipitation are perturbed by a proxy temperature record, in this case
451 the GRIP ice core record (Johnsen et al., 1995). These are input into a positive degree day model to calculate mass
452 balance (Calov and Greve, 2005). Input precipitation values are the same between experiments. To introduce
453 variation between the experiments, temperature varies such that Experiment A is the equivalent of modern day
454 values, Experiment B has values uniformly reduced by 1°C and Experiment C has values uniformly reduced by
455 2°C. All other parameters and forcings are equal between experiments. This simple approach to climate forcing
456 here used for demonstration purposes only, and does not capture the changes to atmospheric and oceanic
457 circulation patterns that occur during a glacial cycle.

458 The maximum extent of ice for each experiment is shown in Figure 6 and the timing of advance and retreat is
459 shown in Figure 7. Potentially unrealistic ice sheets occur in the North Sea, perhaps due to the choice of domain
460 not including the influence of the Fennoscandian ice sheet in this area. As noted above, we do not expect these
461 model runs to fully replicate the reconstructed characteristics of the BIIS (e.g. Clark et al., 2012). However, it is

462 worth noting general, visually-derived, observations regarding the outputs shown in Figure 6. For larger
463 temperature offsets, the ice sheet gets bigger, the timing of maximum extent gets progressively later and the
464 modelled ice sheet gets thicker (Figure 6). In all experiments, there is generally a gradual advance toward the
465 maximum extent followed by retreat (Figure 7). This pattern is interrupted by a later readvance that corresponds
466 to the timing of the Younger Dryas in the GRIP record; this causes ice to regrow over high elevation areas such
467 as Scotland and central Wales. The extent of this readvance increases with decreased temperature offsets between
468 experiments (Figure 7). Smaller readvances, occurring around 16.5 ka also occur (Figure 7).

469 **4.2 Geochronological data**

470 Ice-sheet advance dates were taken from the compilation of Hughes et al. (2016) and gridded to the ice sheet
471 model domain (Figure 4). In total, 61 cells were represented with advance dates (Figure 8A). Considering now
472 ice-sheet retreat (Figure 8B), dates deemed reliable or probably reliable by Small et al. (2017) were used (i.e.
473 those given a ‘traffic light rating’ of green or amber). For the dated advance and retreat locations, the
474 geochronological data in each cell was assigned an error corresponding to that which was reported in the literature.
475 We also compared our results to the ‘likely’ empirical reconstruction of Hughes et al. (2016), based on that of
476 Clark et al. (2012) (Figure 8C), using the minimum and maximum bounding envelopes to assign an error to each
477 cell of the ice sheet grid (Figure 8D). The largest errors occur in the North Sea region, where there is a lack of
478 empirical data (e.g. Figures 8A and B).

479 **4.3 Results**

480 Table 4 shows selected statistics derived by ATAT when comparing the three ice-sheet modelling experiments
481 (Figures 6 and 7) against the three categories of data (Advance, Retreat, Isochrones; Figure 8). wRMSE was not
482 calculated for the DATED isochrone reconstruction, as grid points are distributed evenly and therefore have equal
483 spatial weighting (Table 4). Experiment C produces modelled ice-sheets with the greatest areal extent, and
484 therefore performs best at correctly covering the dated areas (Table 4). However, none of the three experiments
485 perform particularly well when compared with the data or the empirical reconstruction regarding timing and
486 results in high (>2000 year) RMSEs (Table 4). The application of ATAT and the results from these simplified
487 experiments allow us to suggest directions for analysing future experiments.

488 All three experiments produced large RMSEs, in the order of thousands of years, when compared to all three
489 categories of data (Table 4). For advance ages, the three simulations conform to a large number of dated locations
490 (e.g. 72% of ages in Experiments B and C; Table 4). However, the RMSEs of advance ages are high (Table 4).
491 This shows that, while the models perform well at matching the constraint of covering an area in ice after an
492 advance age (Figure 3), the models often glaciates a region much later than required. Advance dates are particularly
493 difficult to obtain from the stratigraphic record, and often there may be a long hiatus between the initial deposition
494 of datable material and the subsequent advance of a glacier. Future experiments with large ensembles should
495 therefore consider the number of advance dates conformed to (rather than the RMSE) as a more robust guide for
496 model performance during ice advance.

497 For the retreat comparisons, the three modelling experiments conform to a larger percentage of sites, seemingly
498 outperforming the empirically-derived DATED reconstruction (Table 4). However, where model-data agreement
499 occurs, the RMSE produced are much higher when the model is compared to the DATED reconstruction. This is

500 due to the reconstruction containing large uncertainties in regions which lack geochronological control (for
501 example in the North Sea, Figure 8). These uncertainties, a product of spatial interpolation across regions with
502 sparse information, are much greater than those associated with individual dates. Figure 9A shows examples of
503 output maps from ATAT which display the spatial pattern of agreement and the magnitude of the difference
504 between Experiment C and the DATED reconstruction. This shows that due to the uncertainty associated with
505 North Sea glaciation, even where the model produces an unrealistic artefact, there is data-model agreement.
506 Furthermore, ATAT produces a map which displays the number of years between data-based and modelled retreat
507 and/or advance (e.g. Figure 9B). Figure 9B, which compares Experiment C to the DATED isochrones, shows that
508 the timing of model-data disagreement is spatially variable. If more modelling simulations were conducted, such
509 maps may reveal regions of reconstruction or particular dates which are difficult to simulate in the model. In such
510 cases, data or model re-evaluation may be required and herein lies the potential utility of this ATAT tool in making
511 sense of ensemble model runs. However, such model-data comparison awaits a full-ensemble simulation which
512 accounts for model uncertainty (e.g. Hubbard et al., 2009).

513 **5. Summary and concluding remarks**

514 Here we present ATAT, an automated timing-accordance tool for comparing ice-sheet model output with
515 geochronological data and empirical ice sheet reconstructions. We demonstrate the utility of ATAT through three
516 simplified simulations of the former British-Irish Ice Sheet. Note that a larger ensemble model of hundreds to
517 thousands of runs is required for model evaluation (e.g. Hubbard et al., 2009). ATAT enables users to quantify
518 the difference between the simulated timing of ice sheet advance and retreat and those from a chosen dataset, and
519 allows production of cumulative ice coverage agreement maps that should help distinguish between less and more
520 promising runs. We envisage that this tool will be especially useful for ice-sheet modellers through justifying
521 model choice from an ensemble, quantifying error and tuning ice-sheet model experiments to fit geochronological
522 data. Ideally, this tool should be used in combination with other evaluation methods, such as fit to relative sea-
523 level records. In the case where locations or regions of data cannot be fit by a model, and all model uncertainty
524 has been accounted for in an ensemble simulation, the comparisons made in ATAT may also highlight that data
525 re-evaluation is necessary. ATAT is supplied as supplementary material to this article.

526 **6. Code Availability**

527 ATAT 1.1 source code is freely distributed under a GNU GPL licence as supplementary material to this paper and
528 can be downloaded from <https://figshare.com/s/38d0fd268684ad0fcc2d>. An example geochronological data grid
529 can also be downloaded as supplementary material. The ice sheet modelling experiments shown here were
530 conducted using the Parallel Ice Sheet Model (<http://pism-docs.org/>). Development of PISM is supported by
531 NASA grant NNX17AG65G and NSF grants PLR-1603799 and PLR-1644277. The geochronological data used
532 is freely available from <https://www.sciencedirect.com/science/article/pii/S0012825216304408#s0105> and
533 <https://doi.pangaea.de/10.1594/PANGAEA.848117>.

534 **6.1. General Instructions**

535 ATAT is written in python, and distributed as both .py script, for use in Python 2, and a .py3 script, for use with
536 Python 3. The tool requires installation of Python and the following freely available Python packages:

- 537 • netCDF4 (<https://pypi.python.org/pypi/netCDF4>)
- 538 • numpy (<http://www.numpy.org/>)
- 539 • scipy (<https://www.scipy.org/>)
- 540 • matplotlib (<https://matplotlib.org/>)
- 541 • matplotlib toolkit basemap (<https://matplotlib.org/basemap/>)

542 ATAT can be run from any Python enabled environment (e.g. IDLE, BASH). Here we provide the following
543 simple instructions for running ATAT in a BASH shell. For numerous runs, a shell script should be created.

544 From the command line, launch the ATAT script using python (“python ATATv1.1.py”). Eight command-line
545 arguments (A1 - A8), separated by a space should then follow.

546 A1 dictates whether deglacial or advance ages are being tested. Type “DEGLACIAL” or “ADVANCE”
547 accordingly.

548 A2 is the path to the geochronological data file(e.g. “/home/ATAT/geochron.nc”)

549 A3 defines whether the model extent is based on thickness or a mask. Type THK or MSK accordingly.

550 A4 is the path to the ice-sheet model output file (e.g. “/home/ATAT/icesheetmodel1.nc”)

551 A5 is the value of the ice-sheet output mask. A value is required even if A3 = THK, but can be any value as it will
552 be ignored.

553 A6 to A8 control output maps. A6 defines whether the output map should consider margin uncertainty, with a
554 value of BORDER or NONE.

555 A7 defines whether the model-data offset map displaces RMSE (option “NONE”) or wRMSE (“WEIGHTED”).

556 A8 specifies which dates are plotted on the difference map, and can be “ALL” for all dates, “COVERED” for
557 those which at some point were covered by ice and “INERROR” to display only those dates where model-data
558 agreement within dating error occurred.

559 An example command would be “python ATATv1.1.py DEGLACIAL /home/ATAT/dated_recon.nc MSK
560 /home/ATAT/experiment1.nc 2 BORDER WEIGHTED INERROR”. ATAT then outputs the two maps and a csv
561 table containing all derived statistics.

562 *Acknowledgements:* This work was supported by the Natural Environment Research Council consortium grant;
563 BRITICE-CHRONO NE/J009768/1. We thank Evan Gowan and Lev Tarasov for their constructive reviews which
564 improved the manuscript.

565 **References**

566 Auriac, A., Whitehouse, P.L., Bentley, M.J., Patton, H., Lloyd, J.M. and Hubbard, A. Glacial isostatic adjustment
567 associated with the Barents Sea ice sheet: a modelling inter-comparison. *Quaternary Science Reviews*, 147, 122-
568 135, 2016.

569 Applegate, P.J., Kirchner, N., Stone, E.J., Keller, K. and Greve, R. An assessment of key model parametric
570 uncertainties in projections of Greenland Ice Sheet behavior. *Cryosphere*, 6(3), 589-606, 2012.

571 Arnold, J.R. and Libby, W.F. Radiocarbon dates. *Science*, 113(2927), 111-120, 1951.

572 Balco, G. Contributions and unrealized potential contributions of cosmogenic-nuclide exposure dating to glacier
573 chronology, 1990–2010. *Quaternary Sci Rev*, 30(1), 3-27, 2011.

574 Bamber, J.L. and Aspinall, W.P.. An expert judgement assessment of future sea level rise from the ice sheets. *Nat*
575 *Clim Change*, 3(4), 424-427, 2013.

576 Bateman, M.D., Evans, D.J., Roberts, D.H., Medialdea, A., Ely, J. and Clark, C.D., The timing and consequences
577 of the blockage of the Humber Gap by the last British– Irish Ice Sheet. *Boreas*. 47(1), 41-61, 2018.

578 Boulton, G. and Hagdorn, M. Glaciology of the British Isles Ice Sheet during the last glacial cycle: form, flow,
579 streams and lobes. *Quaternary Sci Rev*, 25(23), 3359-3390, 2006.

580 Braconnot, P., Harrison, S.P., Kageyama, M., Bartlein, P.J., Masson-Delmotte, V., Abe-Ouchi, A., Otto-Bliesner,
581 B. and Zhao, Y., 2012. Evaluation of climate models using palaeoclimatic data. *Nature Climate Change*, 2(6),
582 417-424, 2012.

583 Briggs, R.D. and Tarasov, L. How to evaluate model-derived deglaciation chronologies: a case study using
584 Antarctica. *Quaternary Sci Rev*, 63, 109-127, 2013.

585 Briggs, R.D., Pollard, D. and Tarasov, L. A data-constrained large ensemble analysis of Antarctic evolution since
586 the Eemian. *Quaternary Sci Rev*, 103, 91-115, 2014.

587 Brown, E.J., Rose, J., Coope, R.G. and Lowe, J.J. An MIS 3 age organic deposit from Balglass Burn, central
588 Scotland: palaeoenvironmental significance and implications for the timing of the onset of the LGM ice sheet in
589 the vicinity of the British Isles. *J Quaternary Sci*, 22(3), 295-308, 2007.

590 Bueler, E.D., Lingle, C.S. and Brown, J. Fast computation of a viscoelastic deformable Earth model for ice-sheet
591 simulations. *Ann Glaciol*, 46(1), 97-105, 2007.

592 Bueler, E. and Brown, J. Shallow shelf approximation as a “sliding law” in a thermomechanically coupled ice
593 sheet model. *J Geophys Res-Earth*, 114(F3), 2009.

594 Calov, R. and Greve, R. A semi-analytical solution for the positive degree-day model with stochastic temperature
595 variations. *J Glaciol*, 51(172), 173-175, 2005.

596 Chiverrell, R.C., Thrasher, I.M., Thomas, G.S., Lang, A., Scourse, J.D., van Landeghem, K.J., Mccarroll, D.,
597 Clark, C.D., Cofaigh, C.Ó., Evans, D.J. and Ballantyne, C.K. Bayesian modelling the retreat of the Irish Sea Ice
598 Stream. *J Quaternary Sci*, 28(2), 200-209, 2013.

599 Clark, C.D., Hughes, A.L., Greenwood, S.L., Jordan, C. and Sejrup, H.P. Pattern and timing of retreat of the last
600 British-Irish Ice Sheet. *Quaternary Sci Rev*, 44, 112-146, 2012.

601 Cornford, S.L., Martin, D.F., Graves, D.T., Ranken, D.F., Le Brocq, A.M., Gladstone, R.M., Payne, A.J., Ng,
602 E.G. and Lipscomb, W.H. Adaptive mesh, finite volume modeling of marine ice sheets. *Journal of Computational*
603 *Physics*, 232(1), 529-549, 2013.

604 DeConto, R.M. and Pollard, D. Contribution of Antarctica to past and future sea-level rise. *Nature*, 531(7596),
605 591-597, 2016.

606 Duller, G.A.T. Single grain optical dating of glacial deposits. *Quaternary Geochronology*, 1(4), 296-304, 2006.

607 Dyke, A.S. An outline of North American deglaciation with emphasis on central and northern Canada.
608 *Developments in Quaternary Sciences*, 2, 373-424, 2004.

609 Dyke, A.S. An outline of North American deglaciation with emphasis on central and northern Canada.
610 *Developments in Quaternary Sciences*, 2, 373-424, 2004.

611 Edwards, T.L., Fettweis, X., Gagliardini, O., Gillet-Chaulet, F., Goelzer, H., Gregory, J.M., Hoffman, M.,
612 Huybrechts, P., Payne, A.J., Perego, M. and Price, S. Effect of uncertainty in surface mass balance-elevation
613 feedback on projections of the future sea level contribution of the Greenland ice sheet. *Cryosphere*, 8(1), 195-208.
614 2014.

615 Fowler, A.C. A sliding law for glaciers of constant viscosity in the presence of subglacial cavitation. In
616 *Proceedings of the Royal Society of London A: Mathematical, Physical and Engineering Sciences*, 407(1832),
617 147-170, 1986.

618 Fretwell, P., Pritchard, H.D., Vaughan, D., Bamber, J.L., Barrand, N.E., Bell, R., Bianchi, C., Bingham, R.G.,
619 Blankenship, D.D., Casassa, G. and Catania, G. Bedmap2: improved ice bed, surface and thickness datasets for
620 Antarctica. *Cryosphere*, 7, 375-393, 2013.

621 Fuchs, M. and Owen, L.A. Luminescence dating of glacial and associated sediments: review, recommendations
622 and future directions. *Boreas*, 37(4), 636-659, 2008.

623 Gasson, E., DeConto, R.M., Pollard, D. and Levy, R.H. Dynamic Antarctic ice sheet during the early to mid-
624 Miocene. *Proceedings of the National Academy of Sciences*, 113(13), 3459-3464, 2016.

625 Golledge, N.R., Levy, R.H., McKay, R.M., Fogwill, C.J., White, D.A., Graham, A.G., Smith, J.A., Hillenbrand,
626 C.D., Licht, K.J., Denton, G.H. and Ackert, R.P. Glaciology and geological signature of the Last Glacial
627 Maximum Antarctic ice sheet. *Quaternary Sci Rev*, 78, 225-247, 2013.

628 Gomez, N., Pollard, D., Mitrovica, J.X., Huybers, P., Clark, P.U. Evolution of a coupled marine ice sheet-sea
629 level model, *J Geophys Res*, 117, F01013, 2012.

630 Gomez, N., Pollard, D. and Mitrovica, J.X. A 3-D coupled ice sheet–sea level model applied to Antarctica through
631 the last 40 ky. *Earth and Planet Sc Lett*, 384, 88-99, 2013.

632 Gowan, E.J. An assessment of the minimum timing of ice free conditions of the western Laurentide Ice Sheet.
633 *Quaternary Sci Rev*, 75, 100-113, 2013.

634 Gregoire, L.J., Payne, A.J. and Valdes, P.J. Deglacial rapid sea level rises caused by ice-sheet saddle collapses.
635 *Nature*, 487(7406), 219-222, 2012.

636 Greve, R. and Hutter, K. Polythermal three-dimensional modelling of the Greenland ice sheet with varied
637 geothermal heat flux. *Ann Glaciol*, 21, 8-12, 1995.

638 Gudmundsson, G.H., Krug, J., Durand, G., Favier, L. and Gagliardini, O. The stability of grounding lines on
639 retrograde slopes. *Cryosphere*, 6, 1497-1505, 2012.

640 Gudmundsson, G.H. Ice-shelf buttressing and the stability of marine ice sheets, *Cryosphere*, 7, 647-655, 2013.

641 Heroy, D.C. and Anderson, J.B. Radiocarbon constraints on Antarctic Peninsula ice sheet retreat following the
642 Last Glacial Maximum (LGM). *Quaternary Sci Rev*, 26(25), 3286-3297, 2007.

643 Heyman, J., Stroeven, A.P., Harbor, J.M. and Caffee, M.W. Too young or too old: evaluating cosmogenic
644 exposure dating based on an analysis of compiled boulder exposure ages. *Earth Planet Sc Lett*, 302(1), 71-80,
645 2011.

646 Hindmarsh, R.C. Consistent generation of ice-streams via thermo-viscous instabilities modulated by membrane
647 stresses. *Geophys Res Lett*, 36(6). 2009.

648 Hubbard, A., Bradwell, T., Golledge, N., Hall, A., Patton, H., Sugden, D., Cooper, R. and Stoker, M. Dynamic
649 cycles, ice streams and their impact on the extent, chronology and deglaciation of the British–Irish ice sheet.
650 *Quaternary Sci Rev*, 28(7), 758-776, 2009.

651 Hughes, A.L., Greenwood, S.L. and Clark, C.D. Dating constraints on the last British-Irish Ice Sheet: a map and
652 database. *J Maps*, 7(1), 156-184, 2011.

653 Hughes, A.L., Clark, C.D. and Jordan, C.J. Flow-pattern evolution of the last British Ice Sheet. *Quaternary Sci*
654 *Rev*, 89, 148-168, 2014.

655 Hughes, A.L., Gyllencreutz, R., Lohne, Ø.S., Mangerud, J. and Svendsen, J.I. The last Eurasian ice sheets—a
656 chronological database and time-slice reconstruction, DATED-1. *Boreas*, 45(1), 1-45, 2016.

657 Hughes, T.J., Is the West Antarctic ice sheet disintegrating? *J. Geophys. Res.*, 78 (33), 7884-7910, 1973.

658 Imbrie, J., Hays, J.D., Martinson, D.G., McIntyre, A., Mix, A.C., Morley, J.J., Pisias, N.G., Prell, W.L.,
659 Shackleton, N.J. The orbital theory of Pleistocene climate: support from a revised chronology of the marine $\delta^{18}O$
660 record. In: Berger, A., Imbrie, J., Hays, H., Kukla, G., Saltzman, B. (Eds.), *Milankovitch and Climate, Part I*. D.
661 Reidel Publishing, Dordrecht, 269–305, 1984.

662 Johnsen, S.J., Dahl-Jensen, D., Dansgaard, W. and Gundestrup, N. Greenland palaeotemperatures derived from
663 GRIP bore hole temperature and ice core isotope profiles. *Tellus B*, 47(5), 624-629, 1995.

664 Kirchner, N., Hutter, K., Jakobsson, M. and Gyllencreutz, R. Capabilities and limitations of numerical ice sheet
665 models: a discussion for Earth-scientists and modelers. *Quaternary Sci Rev*, 30(25), 3691-3704, 2011.

666 Kirchner, N., Ahlkrone, J., Gowan, E.J., Lötstedt, P., Lea, J.M., Noormets, R., von Sydow, L., Dowdeswell, J.A.
667 and Benham, T. Shallow ice approximation, second order shallow ice approximation, and full Stokes models: A
668 discussion of their roles in palaeo-ice sheet modelling and development. *Quaternary Sci Rev*, 147, 136-147, 2016.

669 Kleman, J., Hättestrand, C., Stroeven, A.P., Jansson, K.N., De Angelis, H. and Borgström, I. Reconstruction of
670 Palaeo-Ice Sheets-Inversion of their Glacial Geomorphological Record. In Knight, P.G. (Eds) *Glacier science and*
671 *environmental change*, 192-198, 2006.

672 Larour, E., Seroussi, H., Morlighem, M. and Rignot, E. Continental scale, high order, high spatial resolution, ice
673 sheet modeling using the Ice Sheet System Model (ISSM). *J Geophys Res-Earth*, 117(F1), 2012.

674 Libby, W.F., Anderson, E.C. and Arnold, J.R. Age determination by radiocarbon content: world-wide assay of
675 natural radiocarbon. *Science*, 109(2827), 227-228, 1949.

676 Lingle, C.S. and Clark, J.A. A numerical model of interactions between a marine ice sheet and the solid earth:
677 Application to a West Antarctic ice stream. *J Geophys Res-Oceans*, 90(C1), 1100-1114, 1985.

678 Livingstone, S.J., Cofaigh, C.Ó., Stokes, C.R., Hillenbrand, C.D., Vieli, A. and Jamieson, S.S. Antarctic palaeo-
679 ice streams. *Earth-Sci Rev*, 111(1), 90-128, 2012.

680 Lorenz, E.N. Deterministic Nonperiodic Flow, *J. Atmos. Sci.*, 20, 130-141, 1963.

681 Lowe, J.J. and Walker, M.J. Radiocarbon Dating the Last Glacial-Interglacial Transition (Ca. 14–9 14C Ka Bp)
682 in Terrestrial and Marine Records: The Need for New Quality Assurance Protocols. *Radiocarbon*, 42(1), 53-68,
683 2000.

684 Lowell, T.V., Fisher, T.G., Hajdas, I., Glover, K., Loope, H. and Henry, T. Radiocarbon deglaciation chronology
685 of the Thunder Bay, Ontario area and implications for ice sheet retreat patterns. *Quaternary Sci Rev*, 28(17), 1597-
686 1607, 2009.

687 Lukas, S., Spencer, J.Q., Robinson, R.A. and Benn, D.I. Problems associated with luminescence dating of Late
688 Quaternary glacial sediments in the NW Scottish Highlands. *Quaternary Geochron*, 2(1), 243-248, 2007.

689 Mercer, J.H. West Antarctic ice sheet and CO₂ greenhouse effect: a threat of disaster. *Nature*, 271, 321-325, 1978.

690 Napieralski, J., Harbor, J. and Li, Y. Glacial geomorphology and geographic information systems. *Earth-Sci Rev*,
691 85(1), 1-22, 2007.

692 Ó Cofaigh, C.Ó. and Evans, D.J. Radiocarbon constraints on the age of the maximum advance of the British–Irish
693 Ice Sheet in the Celtic Sea. *Quaternary Sci Rev*, 26(9), 1197-1203, 2007.

694 Patton, H., Hubbard, A., Andreassen, K., Winsborrow, M. and Stroeven, A.P. The build-up, configuration, and
695 dynamical sensitivity of the Eurasian ice-sheet complex to Late Weichselian climatic and oceanic forcing.
696 *Quaternary Sci Rev*, 153, 97-121, 2016.

697 Pattyn, F. Sea-level response to melting of Antarctic ice shelves on multi-centennial timescales with the fast
698 Elementary Thermomechanical Ice Sheet model (f. ETISH v1. 0). *Cryosphere*, 11(4), p.1851-1878, 2017.

699 Pattyn, F., Perichon, L., Aschwanden, A., Breuer, B., De Smedt, B., Gagliardini, O., Gudmundsson, G.H.,
700 Hindmarsh, R., Hubbard, A., Johnson, J.V. and Kleiner, T. Benchmark experiments for higher-order and full
701 Stokes ice sheet models (ISMIP-HOM). *Cryosphere*, 2(1), 111-151, 2008.

702 Pattyn, F., Schoof, C., Perichon, L., Hindmarsh, R.C.A., Bueler, E., Fleurian, B.D., Durand, G., Gagliardini, O.,
703 Gladstone, R., Goldberg, D. and Gudmundsson, G.H. Results of the marine ice sheet model intercomparison
704 project, MISMIP. *Cryosphere*, 6(3), 573-588, 2012.

705 Pollard, D. and DeConto, R.M. Modelling West Antarctic ice sheet growth and collapse through the past five
706 million years. *Nature*, 458(7236), 329-332, 2009.

707 Ritz, C., Edwards, T.L., Durand, G., Payne, A.J., Peyaud, V. and Hindmarsh, R.C. Potential sea-level rise from
708 Antarctic ice-sheet instability constrained by observations. *Nature*, 528(7580), 115-118, 2015.

709 Robinson, A., Calov, R. and Ganopolski, A. Greenland ice sheet model parameters constrained using simulations
710 of the Eemian Interglacial. *Clim Past*, 7(2), 381-396, 2011.

711 Rutt, I.C., Hagdorn, M., Hulton, N.R.J. and Payne, A.J. The Glimmer community ice sheet model. *J Geophys*
712 *Res-Earth*, 114(F2), 2009.

713 Schoof, C.S. Ice sheet grounding line dynamics: steady states, stability and hysteresis. *J. Geophys. Res. Earth*
714 *Surf.*, 112, F03S28, 2007.

715 Schoof, C. Coulomb friction and other sliding laws in a higher-order glacier flow model. *Math Mod Meth Appl*
716 *S*, 20(01), 157-189, 2010.

717 Schoof, C. Marine ice sheet stability. *J. Fluid Mech.*, 698, 62-72, 2012.

718 Seddik, H., Greve, R., Zwinger, T., Gillet-Chaulet, F. and Gagliardini, O. Simulations of the Greenland ice sheet
719 100 years into the future with the full Stokes model Elmer/Ice. *J Glaciol*, 58(209), 427-440, 2012.

720 Seguinot, J., Rogozhina, I., Stroeven, A.P., Margold, M. and Kleman, J. Numerical simulations of the Cordilleran
721 ice sheet through the last glacial cycle. *Cryosphere*, 10, 639-664, 2016.

722 Simpson, M.J., Milne, G.A., Huybrechts, P. and Long, A.J. Calibrating a glaciological model of the Greenland
723 ice sheet from the Last Glacial Maximum to present-day using field observations of relative sea level and ice
724 extent. *Quaternary Sci Rev*, 28(17), 1631-1657, 2009.

725 Small, D., Clark, C.D., Chiverrell, R.C., Smedley, R.K., Bateman, M.D., Duller, G.A., Ely, J.C., Fabel, D.,
726 Medialdea, A. and Moreton, S.G. Devising quality assurance procedures for assessment of legacy
727 geochronological data relating to deglaciation of the last British-Irish Ice Sheet. *Earth-Sci Rev*, 164, 232-250,
728 2017.

729 Smedley, R.K., Glasser, N.F. and Duller, G.A.T. Luminescence dating of glacial advances at Lago Buenos Aires
730 (~ 46° S), Patagonia. *Quaternary Sci Rev*, 134, 59-73, 2016.

731 Smedley, R.K., Chiverrell, R.C., Ballantyne, C.K., Burke, M.J., Clark, C.D., Duller, G.A.T., Fabel, D., McCarroll,
732 D., Scourse, J.D., Small, D. and Thomas, G.S.P. Internal dynamics condition centennial-scale oscillations in
733 marine-based ice-stream retreat. *Geology*, 45(9), 787-790, 2017.

734 Stokes, C.R., Tarasov, L., Blomdin, R., Cronin, T.M., Fisher, T.G., Gyllencreutz, R., Hättestrand, C., Heyman, J.,
735 Hindmarsh, R.C., Hughes, A.L. and Jakobsson, M. On the reconstruction of palaeo-ice sheets: recent advances
736 and future challenges. *Quaternary Sci Rev*, 125, 15-49, 2015.

737 Tarasov, L. and Peltier, W.R. A geophysically constrained large ensemble analysis of the deglacial history of the
738 North American ice-sheet complex. *Quaternary Sci Rev*, 23(3), 359-388, 2004.

739 Tarasov, L., Dyke, A.S., Neal, R.M. and Peltier, W.R. A data-calibrated distribution of deglacial chronologies for
740 the North American ice complex from glaciological modeling. *Earth Planet Sc Lett*, 315, 30-40, 2012.

741 Tushingham, A.M. and Peltier, W.R. Validation of the ICE-3G Model of Würm-Wisconsin Deglaciation using a
742 global data base of relative sea level histories. *J Geophys Res-Solid Earth*, 97(B3), 3285-3304, 1992.

743 Weertman, J. Stability of the junction of an ice-sheet and an ice-shelf. *J. Glaciol.* 13 (67), 3-11, 1974.

744 Winkelmann, R., Martin, M.A., Haseloff, M., Albrecht, T., Bueler, E., Khroulev, C. and Levermann, A. The
745 Potsdam parallel ice sheet model (PISM-PIK)-Part 1: Model description. *Cryosphere*, 5(3), 715-726, 2011.

746

747

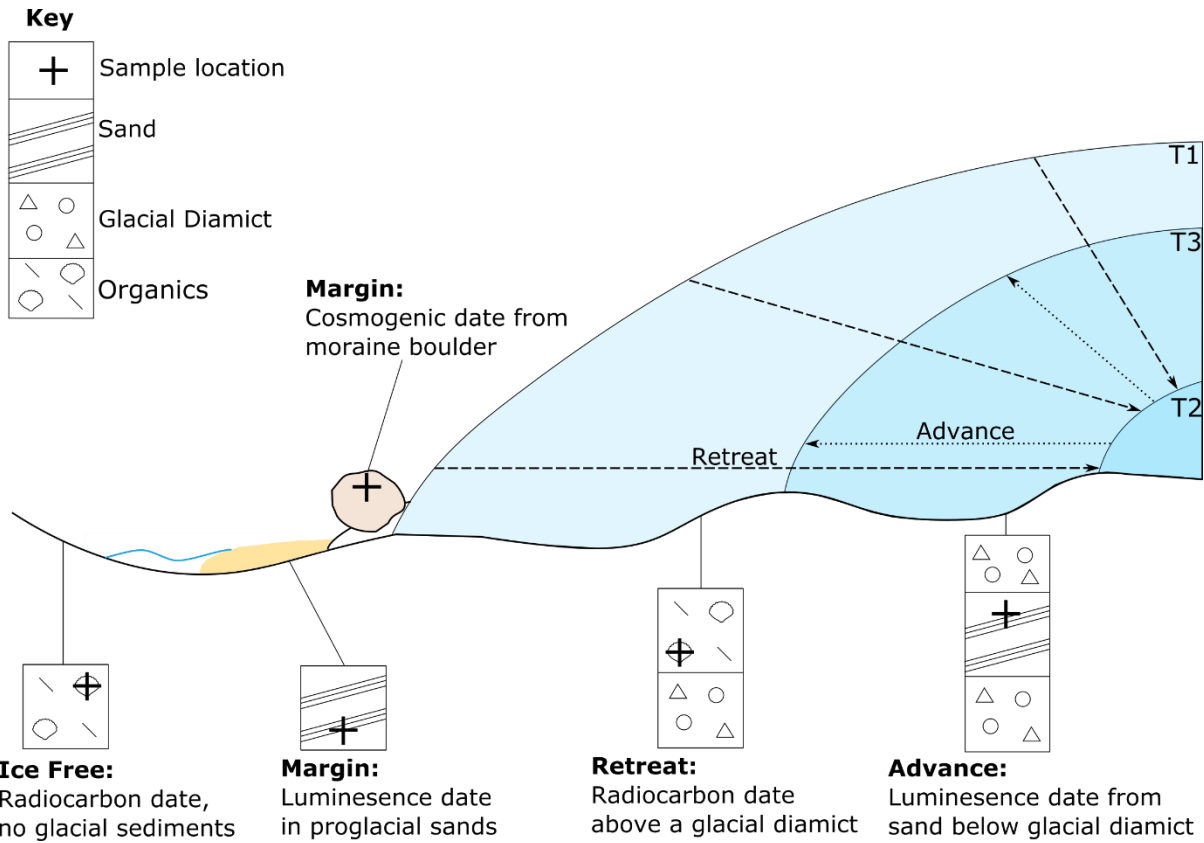
748

749

750

751

752

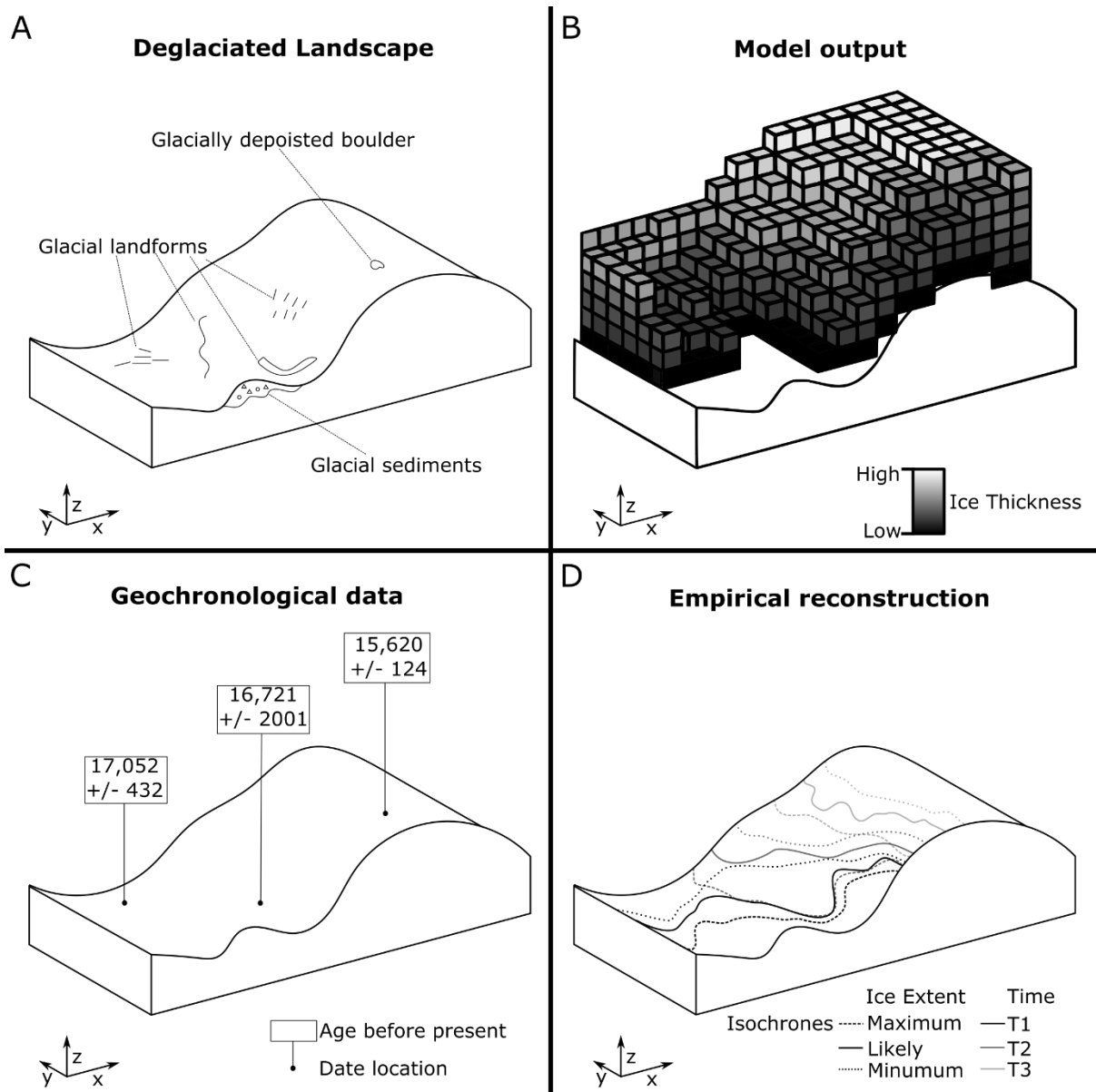


753

754

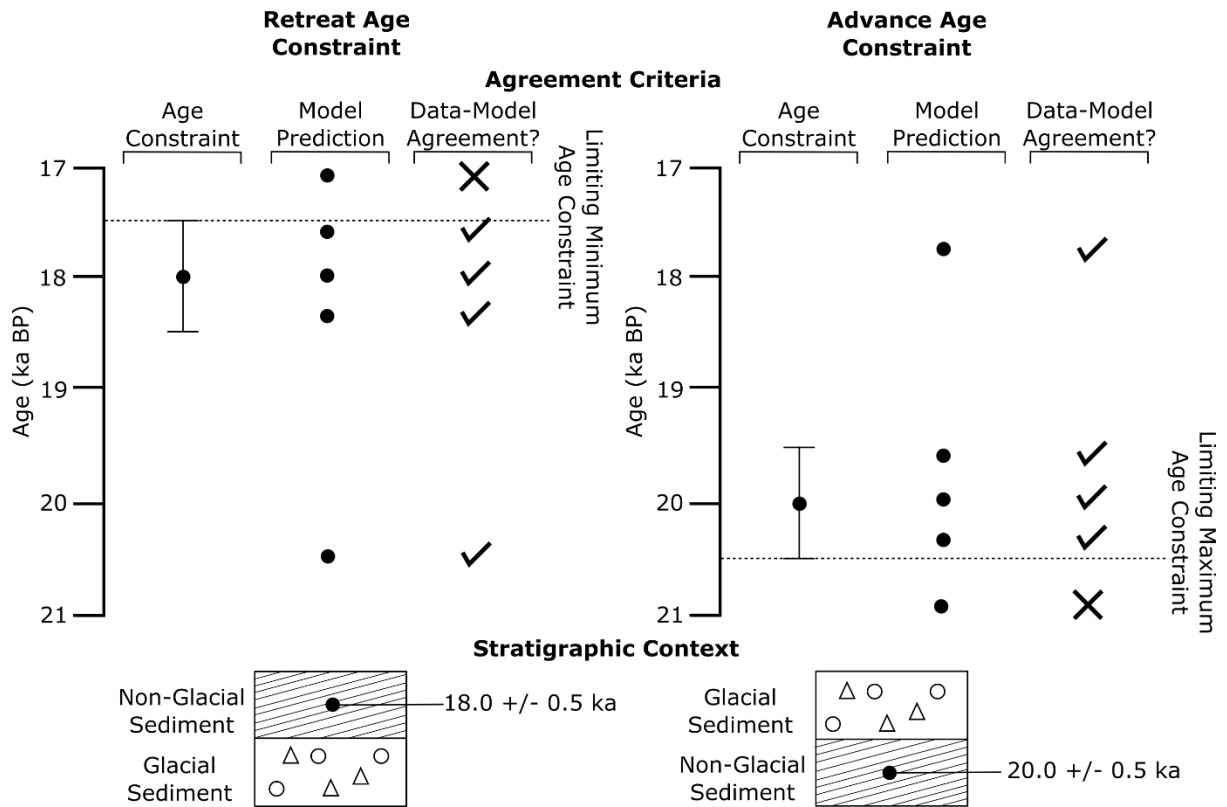
755

Figure 1: Schematic illustration of stratigraphic and inferred glaciological context of geochronological data. Note that at T1 the ice sheet is at its most advanced. It then retreats to a minimum at T2, before re-advancing to T3.



756

757 **Figure 2. Schematic of geochronological data and ice-sheet model output. A) A deglaciaded landscape,**
 758 **demonstrating some of the features used by palaeo-glaciologists when empirically reconstructing an ice**
 759 **sheet. B) Ice-sheet model output, displaying modelled ice-sheet thickness, in this case at a specific time. C)**
 760 **Geochronological data. D) Empirical reconstruction. Note how the nature of these data vary between**
 761 **source.**



762

763

764

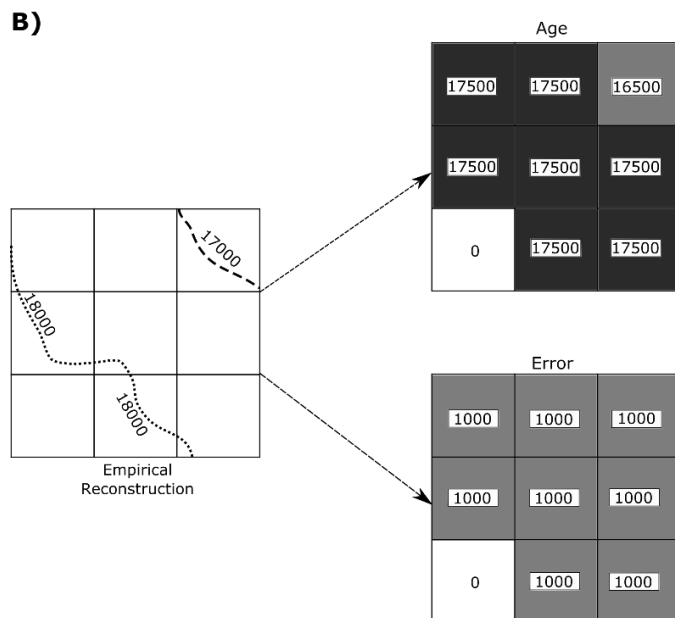
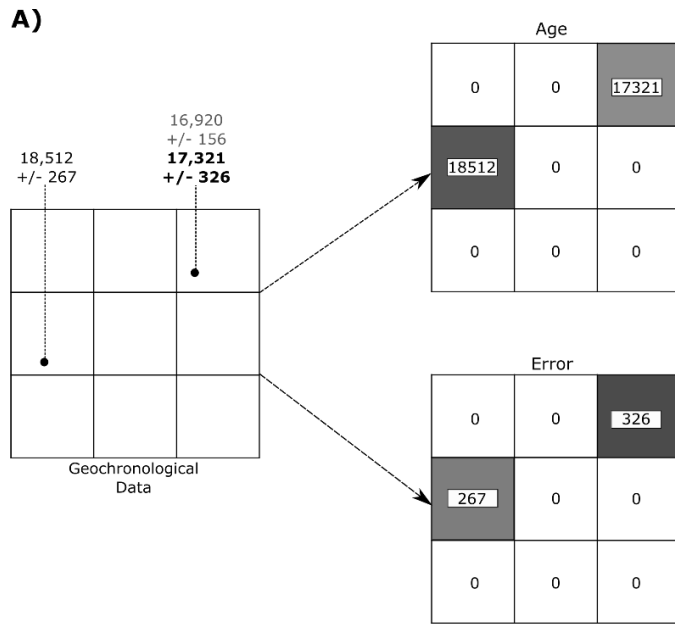
765

766

767

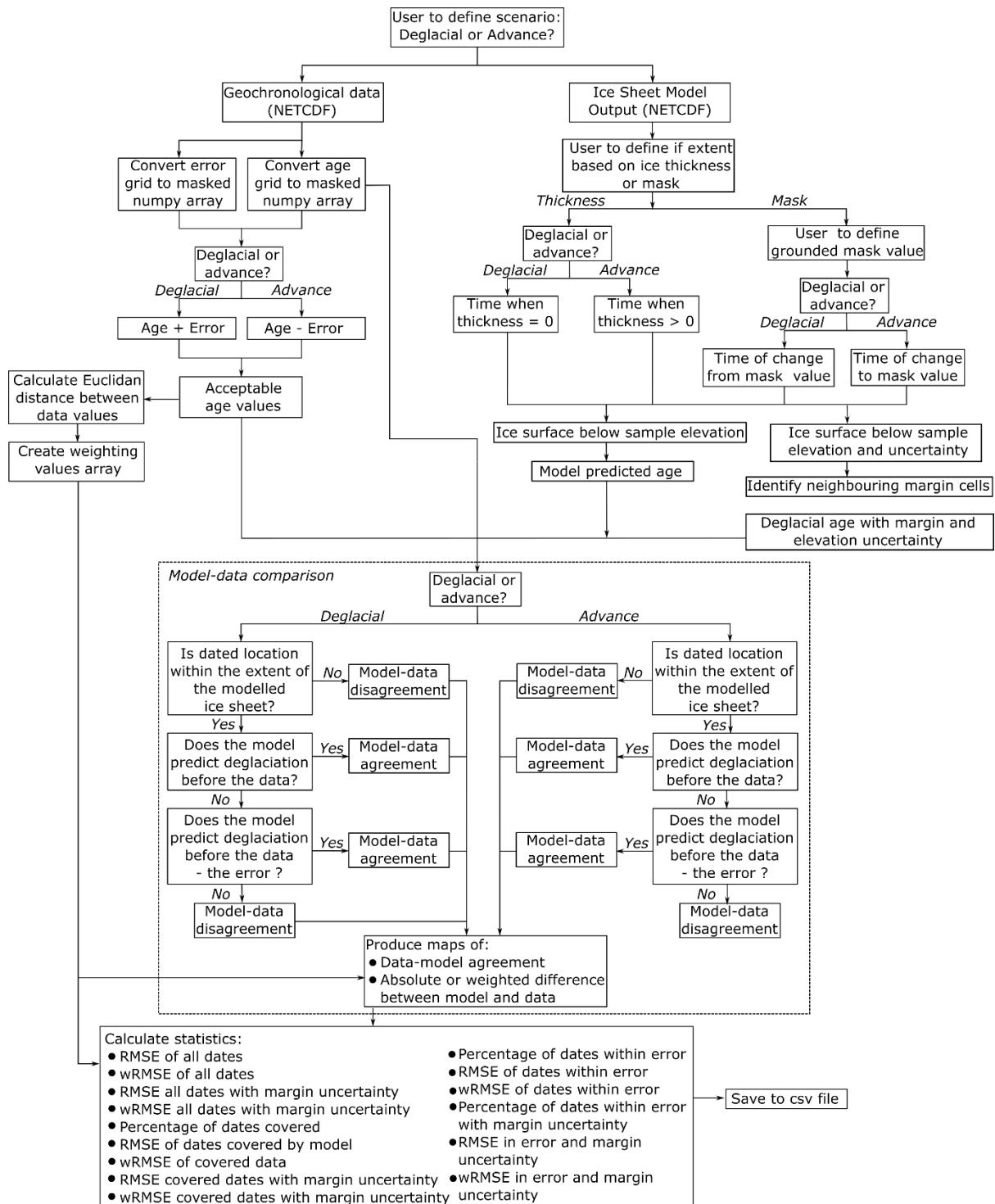
768

Figure 3. Identification of data-model agreement with consideration of error by ATAT for retreat (left) and advance (right) data. If a model predicts ice free conditions before an ice-free age, or during the associated error, there is data-model agreement. If deglaciation occurs at this location after the error, the model disagrees with the data. If a model predicts ice advance and cover before the advance age and its associated error, there is model-data disagreement. Agreement between the model and data occurs if ice advances over the location after the date, or before the date within the range of the error.



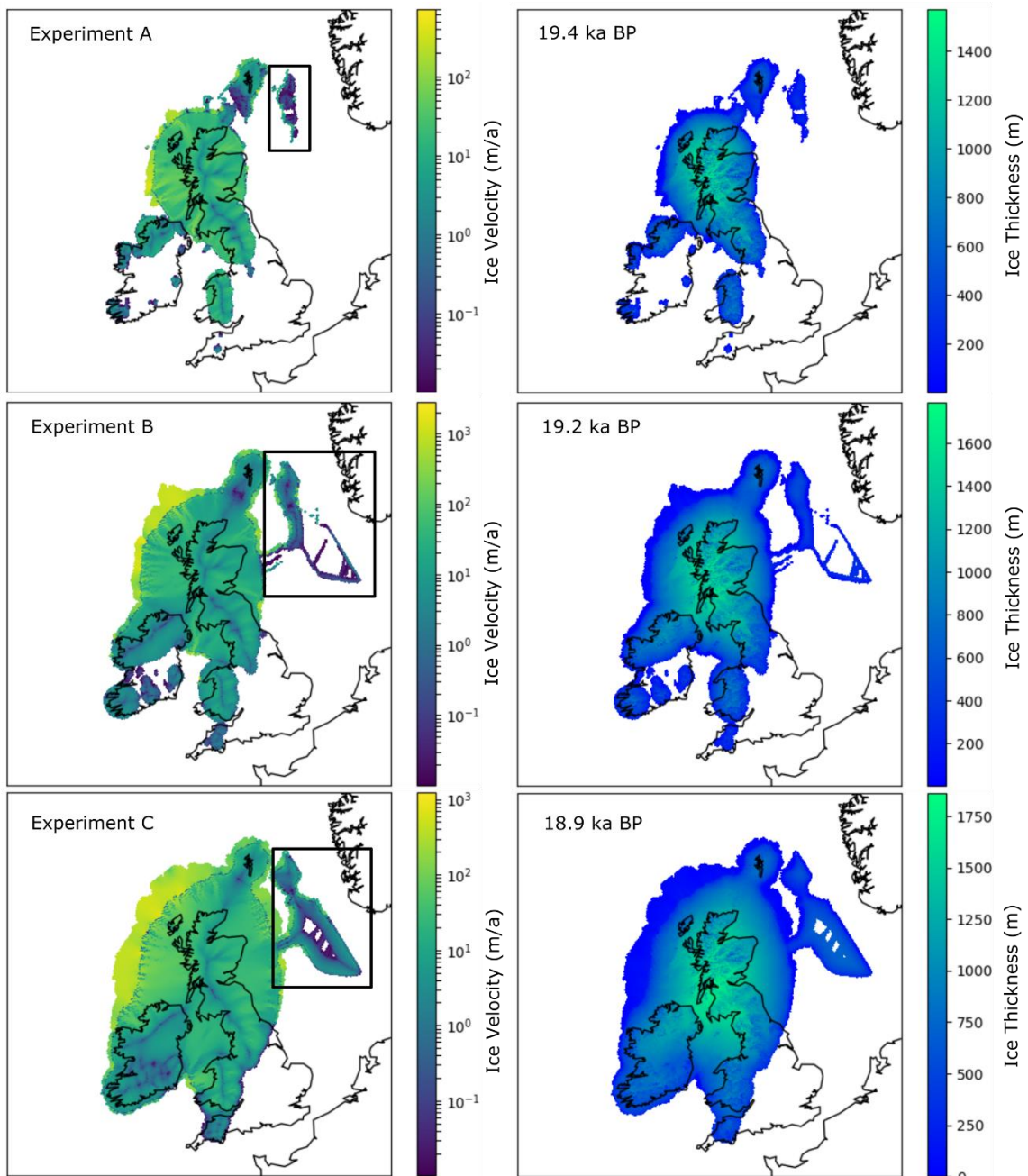
769

770 **Figure 4. Examples of empirical data preparation for ATAT. (A) Conversion of geochronological data into**
 771 **a grid for ATAT. In this example the user has made a judgement based on a priori knowledge that the date**
 772 **of $17,321 \pm 326$ is most representative of the event of interest. Note that age and error are split into separate**
 773 **grids, and that no data regions are assigned a value of 0. (B) Conversion of an empirical reconstruction**
 774 **(margin isochrones) into a grid for ATAT. Here we simply assume that the area between isochrones became**
 775 **deglaciated between at the age between the two isochrones, and that associated error is 1000 years. More**
 776 **complex reconstructions (e.g. Hughes et al., 2016) may require different user-defined rules.**



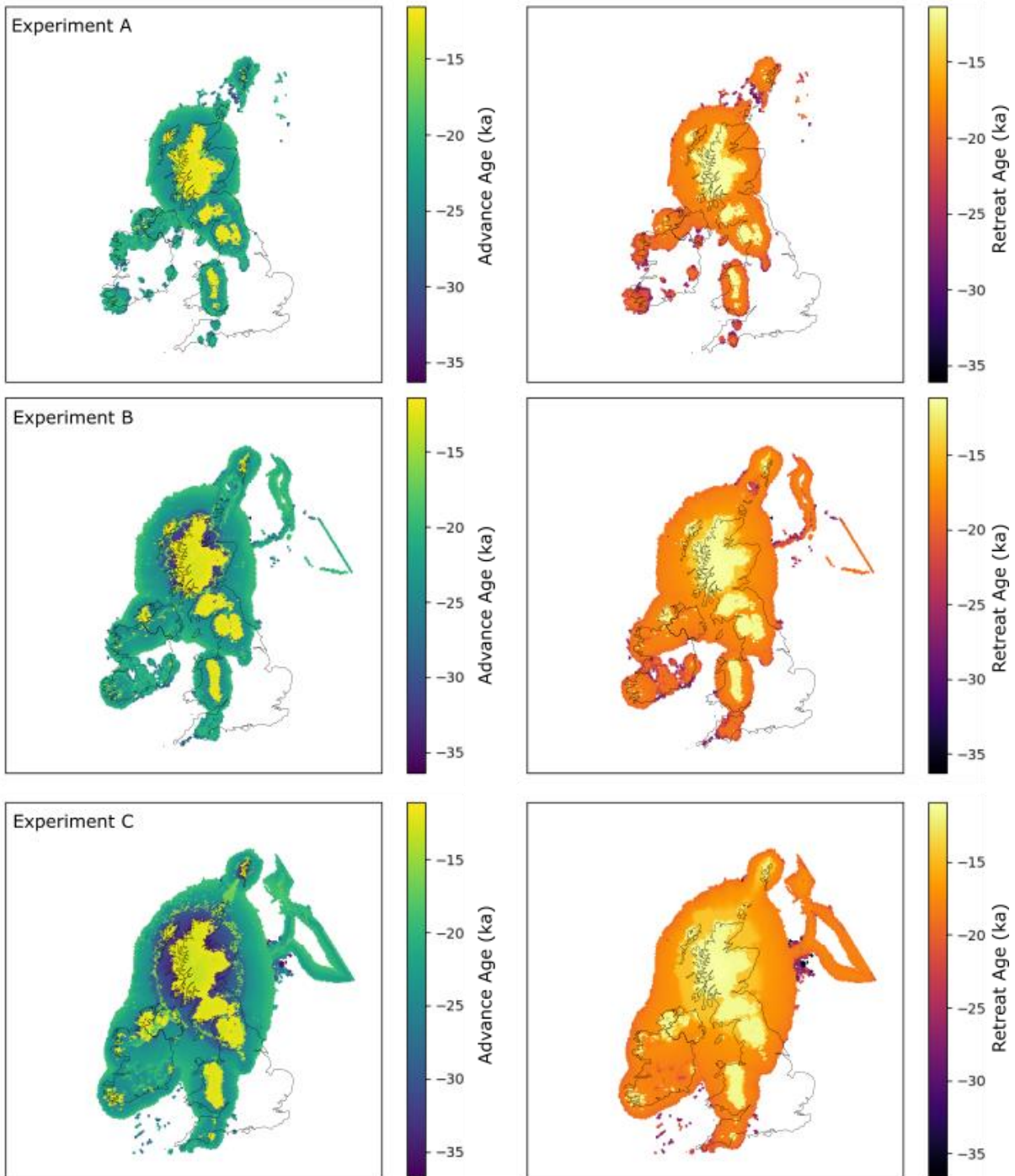
777

778 **Figure 5. Flow chart of ATAT procedure. See text for further description.**



779

780 **Figure 6. Maximum extent of produced ice sheet for the three experiments. Experiment B is 1°C colder**
 781 **than A, and experiment C is 2°C colder than A. Left panel shows ice velocity, right is ice thickness. The box**
 782 **on the left panel highlights likely erroneous output in the North Sea, likely a consequence of model domain,**
 783 **discussed further in the text.**

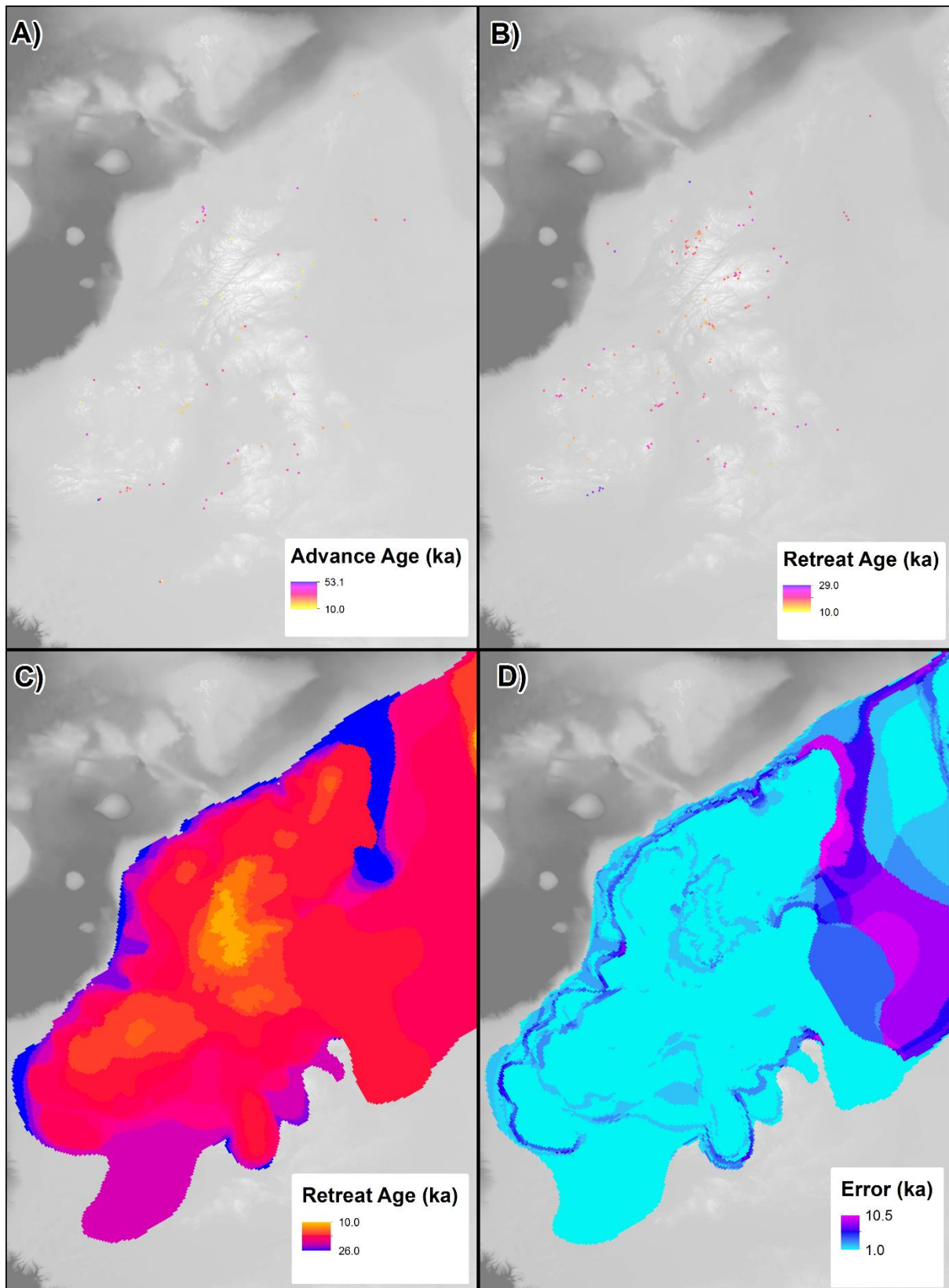


784

785 **Figure 7. Timing of advance (left) and retreat (right) from the three ice sheet modelling experiments.**

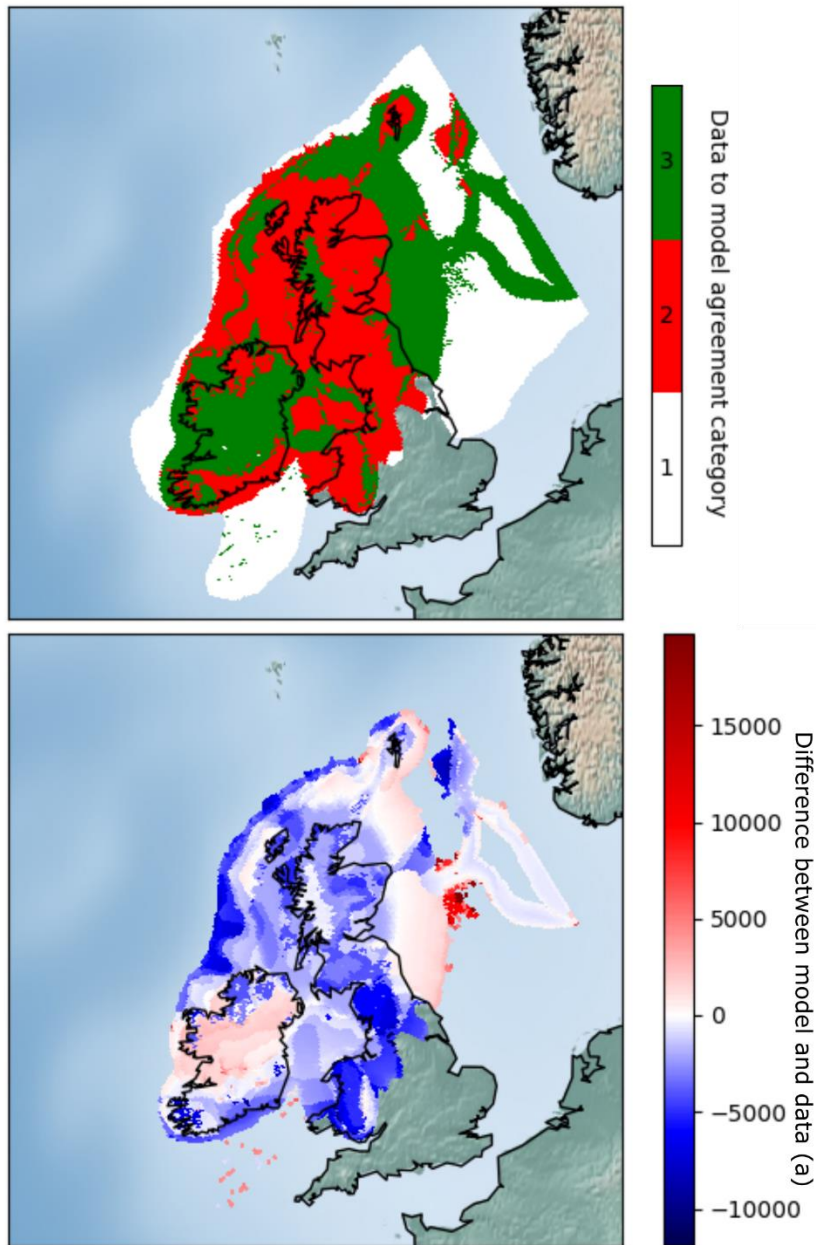
786 **Experiments are the same as in Figure 6. The early ages toward the centre of the model, and centred over**

787 **higher topography, represent the modelled extent of the Younger Dryas readvance.**



788
789
790
791
792

Figure 8. Example of geochronological data projected onto model raster grids; as point-data in A and B and from an empirical reconstruction in C and D. (A). Advance ages from Hughes et al. (2016). (B) Retreat ages from Small et al. (2017). (C) Retreat age derived from DATED isochrone reconstruction (Hughes et al., 2016). (D) Error associated with reconstruction in C.



793

794

795

796

797

798

799

Figure 9. Example mapped outputs from ATAT. In this case, experiment C was compared with the DATED reconstruction. Top map (cumulative agreement) shows categories of data-model agreement across the domain, where 1 = not covered by model, 2 = no agreement and 3 = data-model agreement within error. The lower map (model-data offset) shows magnitude of difference between model and data; negative values show a modelled retreat of ice later than the DATED isochrones, and positive values show a modelled retreat of ice before the DATED isochrones.

800 Table 1. Classification of geochronological data (after Hughes et al., 2011) and its use in ATAT.

Class	Glaciological context	Stratigraphic context	Example	Use in ATAT
Advance	Ice-sheet build up	Material directly below or incorporated within glacial diamict	Luminescence date from a sand below a glacial diamict	Ice cover a short time after this date
Retreat	Ice-free after ice cover	Dated material above glacial diamict	Radiocarbon date of a shell above a glacial diamict	Ice-free conditions from this date onwards (note deglaciation could have occurred a long time before)
Ice Free	Ice-free, but lacking direct information regarding ice	Dated material which indicates ice-free conditions but has no relation to ice cover. It may be much younger and not provide much useful constraint.	Radiocarbon date of organic sediments without underlying glacial sediments	
Margin	Proximal to an ice sheet margin	Dated material with information that ties it to an ice margin	Luminescence date in proglacial sands	
Exposure time (cumulative)	Length of time since sample exposed	N/A	Cosmogenic isotope on erratic boulder above a trimline	Not used

801

Table 2. Comparison of attributes between geochronological data and ice sheet model output.

	Nature of data produced	Spatial resolution	Spatial continuity	Temporal frequency and resolution	Sources of uncertainty	Main limitation
Geochronological data	Timing of the absence of ice at a location	Point location	Point location, unevenly distributed in space, but can be interpolated	Determined by data availability and associated error	Instrumental, environmental and stratigraphic factors	Reliant upon correct stratigraphic interpretation to tie to glaciological events
Ice-sheet model output	Simulation of physically plausible ice sheet conditions	Various, ranging from tens to unit kilometres.	Spatially even, regularly-spaced across entire domain	Continuous in time. Precise subannual resolution possible, but not recorded in practice	Parameterisations, boundary conditions	Based upon mathematical and physical approximations of ice flow

Data source	NetCDF Variable	Units	Dimensions	Description	Notes
		Time	unit x, y	Calendar years before present	
		before reference calendar date			
Ice sheet model output	thk	m	time, x,y	Ice thickness	Either “thk” or “msk” required by ATAT.
	msk	Integers	time, x,y	Grounded/floating/icefree mask	Either “thk” or “msk” required by ATAT. User defines value referring to the location of grounded ice
	lat	Decimal degrees	x, y	Latitude	
Both	lon	Decimal degrees	x, y	Longitude	
Geochronological data	age	Time	unit x, y	Timing of deglaciated conditions	Deglacial and advance ages must be in separate files.
		before reference calendar date			
	error	Seconds	x, y	Error associated with deglaciated conditions	Error associated with either deglacial and advance age must be in associated separate file.
	topg	m	x,y	Modern elevation at resolution of ice-sheet model	

elevation m x,y Elevation of collected sample

Table 3. Required input variables for ATAT NetCDF files.

Table 4: Example statistics from ATAT. Note that the RMSE is often altered by applying the spatial weighting to create wRMSE.

	Advance			Retreat			Empirical Reconstruction; DATED		
Ice Sheet Modelling Experiment	A	B	C	A	B	C	A	B	C
Percentage of dates covered	52.5	72.1	88.5	76.1	91.7	96.3	32.9	52.6	69.8
Percentage that agree within error	65.6	72.7	72.2	22.0	22.0	12.8	23.2	27.0	17.8
RMSE dates covered by model	11075.9	12732.7	13490.3	3879.0	4180.9	4945.4	2972.5	2678.0	2920.8
wRMSE dates covered by model	13357.3	13994.7	14849.7	4073.4	4450.3	5165.8	N/A	N/A	N/A
RMSE dates within error	655.7	478.6	289.3	403.6	259.7	236.2	12023.4	10638.7	8777.6
wRMSE dates within error	615.4	395.0	223.6	422.1	276.9	248.9	N/A	N/A	N/A